NASA TN D-691

TECHNICAL NOTE

D-691

STUDY OF SYSTEMS USING INERTIA WHEELS FOR PRECISE ATTITUDE CONTROL OF A SATELLITE

By John S. White and Q. Marion Hansen

Ames Research Center
Moffett Field, Calif.

NATIONAL AERONAUTICS AND SPACE ADMINISTRATION
WASHINGTON
April 1961

TABLE OF CONTENTS

NATIONAL AERONAUTICS AND SPACE ADMINISTRATION

TECHNICAL NOTE D-691

STUDY OF SYSTEMS USING INERTIA WHEELS FOR PRECISE ATTITUDE CONTROL OF A SATELLITE

By John S. White and Q. Marion Hansen

SUMMARY

Systems using inertia wheels are evaluated in this report to determine their suitability for precise attitude control of a satellite and to select superior system configurations. Various possible inertia wheel system configurations are first discussed in a general manner. Three of these systems which appear more promising than the others are analyzed in detail, using the Orbiting Astronomical Observatory as an example. The three systems differ from each other only by the method of damping, which is provided by either a rate gyro, an error-rate network, or a tachometer in series with a high-pass filter.

An analytical investigation which consists of a generalized linear analysis, a nonlinear analysis using the switching-time method, and an analog computer study shows that all three systems are theoretically capable of producing adequate response and also of maintaining the required pointing accuracy for the Orbiting Astronomical Observatory of ±0.1 second of arc. Practical considerations and an experimental investigation show, however, that the system which uses an error-rate network to provide damping is superior to the other two systems. The system which uses a rate gyro is shown to be inferior because the threshold level causes a significant amount of limit-cycle operation, and the system which uses a tachometer with a filter is shown to be inferior because a device with the required dynamic range of operation does not appear to be available. The experimental laboratory apparatus used to investigate the dynamic performance of the systems is described, and experimental results are included to show that under laboratory conditions with relatively large extraneous disturbances, a dynamic tracking error of less than ±0.5 second of arc was obtained.

INTRODUCTION

For many satellites some form of attitude control is required and, in some cases, the control must be fairly precise. The use of inertia wheels for precise control of satellite attitude is one of the more promising methods within the capabilities of present production and is the subject of this report. Various possible methods of damping will be

considered, and the destabilizing effect of an integrator, which is used to keep the error small, will be examined. After a brief general discussion, the three most promising systems will be analyzed in detail by means of linear and nonlinear analyses, analog computer studies, and laboratory experiments. The three systems differ only by the method of damping, which is provided by either a rate gyro, an error-rate network, or a tachometer in series with a high-pass filter.

The requirements placed on satellite attitude control systems vary from one satellite to another; however, it can be stated generally that a reference, or tracking line, in the satellite is required to be maintained in alinement with a specified external reference, or line of sight, to a specified accuracy, in the presence of disturbing torques and of motion of the external reference. For a stellar or solar pointing satellite, motion of the external reference will be oscillatory at the orbital period, as a result of parallax or velocity aberration. For an earth-pointing satellite the external reference will have a constant velocity. The most significant disturbing torques acting on an earth satellite will probably come from the earth's gravity gradient, the sun's radiation pressure, the earth's atmospheric density, and the earth's magnetic field.

An earth satellite which will suffice as an example for evaluating control systems in this report is the Orbiting Astronomical Observatory. The most stringent fine control requirements presently contemplated for the OAO demand that the pointing error be maintained at less than 0.1 second of arc for one orbital period of approximately 100 minutes. Furthermore, roll motion about the line of sight must be maintained at less than 1 second of arc per second. For stellar sighting the line-of-sight velocity will have a maximum of 0.005 second of arc per second, predominantly from velocity aberration effects. It is expected that the disturbance torques will be on the order of 100 dyne centimeters. A brief description of velocity and torque inputs is included in appendix A, and a more complete discussion may be found in reference 1.

NOTATION

Torque constants (dyne cm/(radian/sec)):

B_e back emf

B_f motor friction

B_m magnetic field

Inertias (gram cm^2):

J_b satellite body

J_w motor and wheel

Gains:

K_a motor amplifier, volts/volt

K_e error amplifier, volts/volt

K_g rate gyro, volts/(radian/sec)

K_i error-rate network, volts/(volt/sec)

K_m motor, (radians/sec)/volt

K_s sensor, volts/radian

A 4 1 8

K_t tachometer with lead network, volts/(radian/sec^2)

K_e' outer loop, $K_s K_e K_a K_m \frac{J_w}{J_b}$, (radians/sec)/radian

K_g' gyro loop, $K_g K_a K_m \frac{J_w}{J_b}$, radians/radian

K_i' error-network loop, $K_s K_i K_a K_m \frac{J_w}{J_b}$, radians/radian

K_t' tachometer loop, $K_t K_a K_m$, radians/(radian/sec)

Time intervals (sec):

t time

t_c control time

t_s settling time to within specified error limit

t_{sw} switching or reversal time of applied motor voltage

$t_{\Delta\varphi_e}$ incremental error time, or time for error to change from one point of zero velocity to the next

Torques (dyne cm):

T_d externally applied disturbance to satellite body

T_{dw} externally applied disturbance to motor and wheel

T_m motor and wheel output

T_{ms} motor output at stall

Voltages (volts):

V applied to motor amplifier

V_m applied to motor

Fictitious block diagram voltages (radians/sec):

V' $K_a K_m \frac{J_w}{J_b} V$

V_m' $K_m \frac{J_w}{J_b} V_m$

Generalized parameters:

ζ damping ratio for second-order equation

τ_1 time constant associated with line-of-sight inputs, sec

τ_2 time constant associated with torque inputs, sec

ω_n natural frequency, radians/sec

Time constants (sec):

τ_d lag in error-rate network

τ_m motor and wheel

τ_t lag in the lead network in series with the tachometer

Angular positions (radians):

φ_b satellite body position

φ_c command or input

φ_e instantaneous error

φ_{eo} initial value of φ_e

φ_{e1} linear range of sensor, or error at which sensor output becomes limited

φ_{ess} steady-state error

$\Delta\varphi_e$ incremental error change during $t_{\Delta\varphi_e}$

Angular velocities (radians/sec):

ω_b instantaneous satellite body relative to inertial space

ω_r roll about line of sight relative to inertial space

ω_w instantaneous motor and wheel relative to inertial space

ω_{wb} instantaneous motor and wheel relative to satellite body

ω_{wo} initial value of ω_w

ω_{ls} line of sight relative to inertial space

SYSTEM CONFIGURATIONS AND ERROR CONSIDERATIONS

System Configurations

A qualitative discussion of system configurations is warranted in order to select systems for further investigation. A rather generalized block diagram of a control system using a motor and inertia wheel for momentum storage is given in sketch (a).

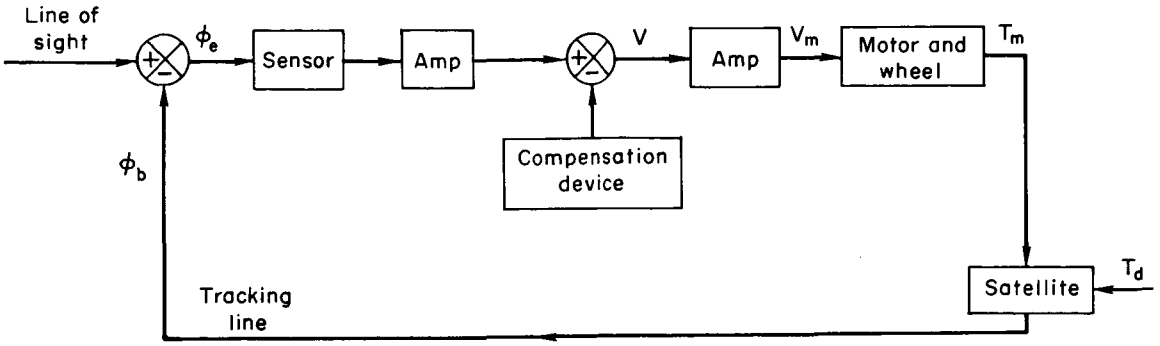

General system diagram

Sketch (a)

The basic system consists of a sensor, appropriate amplifiers, a compensation device, and a motor-wheel combination. An external disturbing torque, T_d, is shown acting on the satellite. When a voltage is applied to the motor, a torque acts directly on the wheel and reacts directly on the satellite body. For simplicity in the remainder of the discussion, the motor is assumed to have a linear torque-speed relationship; that is, the voltage required for constant torque output increases linearly with speed. Such a torque-speed relationship is characteristic of a servomotor.

If no compensation is used, the transient response of the system will be oscillatory, with the amount of damping determined by the time constant of the motor-wheel combination. For the satellite control systems considered, the time constant will be large (since there will be a large wheel on a small motor), so that the system damping will be extremely small. Accordingly, some sort of rate device must be used to damp the system. Such damping can come from a rate gyro, an error-rate network, or a tachometer. The steady-state errors that result from a disturbance torque or a line-of-sight velocity may be analyzed by considering the type of compensation used.

First, consider the effect of a constant disturbance torque, T_d, on an uncompensated system. This torque must be canceled by an equal and opposite constant torque, T_m, from the servomotor if the satellite is to be maintained at a fixed orientation. For an uncompensated system the steady torque from the motor will accelerate the wheel at a constant rate, and the motor voltage will rise linearly as the wheel velocity increases. Thus, in a properly controlled system, a steady-state disturbing torque will cause a constantly increasing motor drive voltage and, also, a constantly increasing error.

If, now, damping is added by means of a rate gyro, the error will be essentially the same as for the uncompensated system because the satellite orientation is nearly constant in the steady state and the gyro signal is approximately zero. The same is true for a damping signal from an error-rate network. If, however, a tachometer is used for damping, the tachometer voltage will increase with wheel velocity. The error signal must overcome this additional voltage to maintain control so that there is a further, and possibly very large, increase in error.

Next, consider the effect of a step change in the line-of-sight velocity, ω_{1s}, on an uncompensated system. For proper tracking, the steady-state satellite angular velocity, ω_b, must equal ω_{1s}. The torque to produce the required ω_b comes from the reaction of the satellite to a corresponding change in the wheel speed, ω_w. Since, in the steady state, the motor voltage increases with ω_w, the result of a step input of angular velocity of the line of sight will be a change in the steady-state motor voltage, V_m, and therefore a corresponding change in the error, φ_e.

The addition of an error-rate network has no effect on the error resulting from a line-of-sight velocity input, since the rate of change of the error is zero in the steady state. However, with the addition of either a rate gyro or a tachometer for damping, a step change in ω_{1s} causes a change in gyro or tachometer voltage which adds, perhaps significantly, to the error.

Summarizing, it is noted that damping by an error-rate network does not increase the steady-state errors for either torque disturbances or line-of-sight velocity inputs, whereas the rate gyro adds to the steady-state error for line-of-sight velocity inputs, and tachometer damping

adds to the errors for both torque disturbances and line-of-sight velocity inputs. In the case of a stellar-pointing satellite, however, line-of-sight velocity inputs are likely to be small, so that the gyro system's deficiency in this respect may not be important. For a system using a tachometer, the increase in steady-state error with wheel velocity can be compensated for by putting a high-pass network, or lead network, after the tachometer in order to pass high frequencies to provide stability during transient conditions and to cut off the lower frequencies to reduce the error during steady-state conditions.

For all three systems discussed thus far, the steady-state error is constant for a constant line-of-sight velocity input, and is steadily increasing for a constant disturbance torque input. The steadily increasing error looks like a serious handicap, but actually, it is not. As was previously shown, this error is necessary in order to force the motor to increase in speed to absorb the momentum from the external torque, and the error is proportional to the momentum. The motor-wheel unit has a maximum amount of momentum which it can absorb; therefore, there is a maximum error that can build up. To maintain continuous control of the satellite in the presence of a steady torque, provisions must be made for removing momentum which has been stored in the wheel. (Jet control would be one way of doing this.) The system must, then, be designed so that it can drive the wheel to maximum momentum without the error exceeding tolerable limits. This can be done in the systems previously discussed either by having sufficient gain or by adding an integrator between the sensor and the motor.

If the integration is provided in the form of an integrating gyro, the maximum torque required from the motor will be much larger than would be required if no integrator were present, as shown in appendix B. If the integrator is electronic, it will require either a larger motor or a considerably larger amount of rate feedback, depending upon its location. One further possibility for integration would be to use a sampling integrator which would sample the error at periods which were long compared to the natural period of the system, but short compared to the time between momentum dumps. Such a system would have essentially no effect on the design, except to reduce the forward loop gain required. A reduction of the forward loop gain, however, would have the perhaps undesirable effect of lengthening the response time. In any case, since the error can be kept sufficiently small without integration in any form, it seems reasonable to select only the three simpler systems for study. Accordingly, the present report is devoted to a theoretical and experimental evaluation of the three systems previously mentioned which provide damping with no integration of any form. These three systems will be referred to in the remainder of this report as the rate-gyro, error-network, and tachometer systems; the tachometer system includes a high-pass filter.

Complete Error Equations

Error equations for the three systems will now be derived. In the derivations, the following simplified motor-wheel transfer function will be used:

$$\frac{T_m}{V_m} = \frac{K_m J_w s}{1 + \tau_m s} \tag{1}$$

A complete block diagram of the motor-wheel combination is included in appendix C with a brief discussion of the simplifications which led to the form used here.

The rate-gyro system is illustrated in sketch (b). Here, it is assumed that the dynamics associated with the gyro may be neglected.

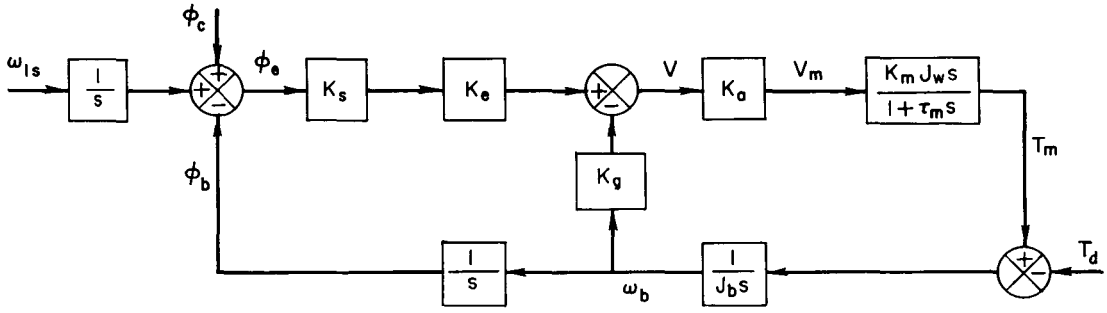

Rate-gyro system

Sketch (b)

The error equation is derived as follows:

The open-loop equation for the inner loop is

$$\omega_b = \frac{K_a K_m \frac{J_w}{J_b} V}{1 + \tau_m s} - \frac{T_d}{J_b s} \tag{2}$$

Substituting the equation,

$$V = K_s K_e \varphi_e - K_g \omega_b \tag{3}$$

and solving for ω_b gives

$$\omega_b = \frac{K_s K_e K_a K_m \frac{J_w}{J_b} \varphi_e - \frac{T_d}{J_b s}(\tau_m s + 1)}{\tau_m s + 1 + K_g K_a K_m \frac{J_w}{J_b}} \tag{4}$$

Using the equation,

$$\omega_b = s\varphi_c + \omega_{1s} - s\varphi_e \tag{5}$$

and solving for φ_e gives

$$\varphi_e = \frac{(s\varphi_c + \omega_{1s})\left(s + \frac{1}{\tau_m} + \frac{K_g K_a K_m \frac{J_w}{J_b}}{\tau_m}\right) + \frac{T_d}{J_b s}\left(s + \frac{1}{\tau_m}\right)}{s^2 + \left(\frac{1}{\tau_m} + \frac{K_g K_a K_m \frac{J_w}{J_b}}{\tau_m}\right) s + \frac{K_s K_e K_a K_m \frac{J_w}{J_b}}{\tau_m}} \tag{6}$$

A
4
1
8

or, expressed with loop gains combined into single symbols as defined in the Notation section,

$$\varphi_e = \frac{(s\varphi_c + \omega_{1s})\left(s + \frac{1}{\tau_m} + \frac{K_g'}{\tau_m}\right) + \frac{T_d}{J_b s}\left(s + \frac{1}{\tau_m}\right)}{s^2 + \left(\frac{1}{\tau_m} + \frac{K_g'}{\tau_m}\right) s + \frac{K_e'}{\tau_m}} \tag{7}$$

The error-network system is illustrated in sketch (c).

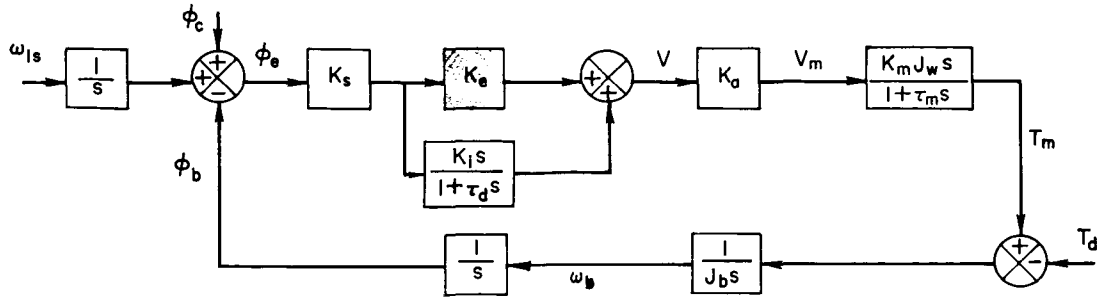

Error-network system

Sketch (c)

The open-loop equation may be written as

$$\omega_b = \frac{K_s \left(K_e + \frac{K_i s}{1 + \tau_d s} \right) K_a K_m \frac{J_w}{J_b} \varphi_e}{1 + \tau_m s} - \frac{T_d}{J_b s} \tag{8}$$

Using equation (5) and solving for φ_e as before gives

$$\varphi_e = \frac{\left(s\varphi_c + \omega_{1s} + \frac{T_d}{J_b s} \right) \left[s^2 + \left(\frac{1}{\tau_d} + \frac{1}{\tau_m} \right) s + \frac{1}{\tau_d \tau_m} \right]}{s^3 + \left(\frac{1}{\tau_d} + \frac{1}{\tau_m} \right) s^2 + \left(\frac{1}{\tau_d \tau_m} + \frac{K_s K_e K_a K_m \frac{J_w}{J_b}}{\tau_m} + \frac{K_s K_i K_a K_m \frac{J_w}{J_b}}{\tau_d \tau_m} \right) s + \frac{K_s K_e K_a K_m \frac{J_w}{J_b}}{\tau_d \tau_m}} \tag{9}$$

A4188

or, expressed with loop gain symbols,

$$\varphi_e = \frac{\left(s\varphi_c + \omega_{1s} + \frac{T_d}{J_b s} \right) \left[s^2 + \left(\frac{1}{\tau_d} + \frac{1}{\tau_m} \right) s + \frac{1}{\tau_d \tau_m} \right]}{s^3 + \left(\frac{1}{\tau_d} + \frac{1}{\tau_m} \right) s^2 + \left(\frac{1}{\tau_d \tau_m} + \frac{K_e'}{\tau_m} + \frac{K_i'}{\tau_d \tau_m} \right) s + \frac{K_e'}{\tau_d \tau_m}} \tag{10}$$

The tachometer system is illustrated in sketch (d).

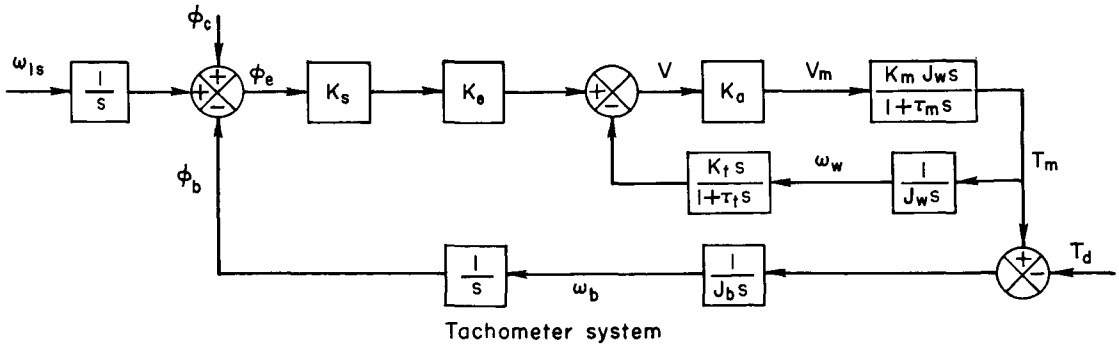

Tachometer system

Sketch (d)

The open-loop equation for the inner loop is

$$T_m = \frac{K_a K_m J_w s V}{1 + \tau_m s} \tag{11}$$

Substituting the equation,

$$V = K_s K_e \varphi_e - \frac{\frac{K_t}{J_w}}{1 + \tau_t s} T_m \tag{12}$$

and solving for T_m gives

A
4
1
8

$$T_m = \frac{K_s K_e K_a K_m J_w s(\tau_t s + 1)\varphi_e}{\tau_t \tau_m s^2 + (\tau_t + \tau_m + K_t K_a K_m)s + 1} \tag{13}$$

Using the equation,

$$T_m = J_b s(s\varphi_c + \omega_{1s} - s\varphi_e) + T_d \tag{14}$$

and solving for φ_e gives

$$\varphi_e = \frac{\left(s\varphi_c + \omega_{1s} + \frac{T_d}{J_b s}\right)\left[s^2 + \left(\frac{1}{\tau_t} + \frac{1}{\tau_m} + \frac{K_t K_a K_m}{\tau_t \tau_m}\right)s + \frac{1}{\tau_t \tau_m}\right]}{s^3 + \left(\frac{1}{\tau_t} + \frac{1}{\tau_m} + \frac{K_t K_a K_m}{\tau_t \tau_m}\right)s^2 + \left(\frac{1}{\tau_t \tau_m} + \frac{K_s K_e K_a K_m \frac{J_w}{J_b}}{\tau_m}\right)s + \frac{K_s K_e K_a K_m \frac{J_w}{J_b}}{\tau_t \tau_m}} \tag{15}$$

or, expressed with loop-gain symbols,

$$\varphi_e = \frac{\left(s\varphi_c + \omega_{1s} + \frac{T_d}{J_b s}\right)\left[s^2 + \left(\frac{1}{\tau_t} + \frac{1}{\tau_m} + \frac{K_t'}{\tau_t \tau_m}\right)s + \frac{1}{\tau_t \tau_m}\right]}{s^3 + \left(\frac{1}{\tau_t} + \frac{1}{\tau_m} + \frac{K_t'}{\tau_t \tau_m}\right)s^2 + \left(\frac{1}{\tau_t \tau_m} + \frac{K_e'}{\tau_m}\right)s + \frac{K_e'}{\tau_t \tau_m}} \tag{16}$$

Steady-State Error Equations

The steady-state errors resulting from φ_c, ω_{1s}, and T_d for the three systems can be readily calculated if the final value theorem is applied to the error equations just derived (eqs. (7), (10), and (16)).

For a step position input of $\varphi_c(s) = \varphi_c/s$ (with $\omega_{1s} = T_d = 0$), the final value or steady-state error is seen to be zero for all three systems, since

$$\frac{\varphi_{ess}}{\varphi_c} = \lim_{s \to 0} s\varphi_e(s) = 0 \tag{17}$$

However, for a ramp position or step velocity input, $\omega_{1s}(s) = \omega_{1s}/s$ (with $\varphi_c = T_d = 0$), the three systems have the following steady-state errors:

Rate-gyro system:

$$\frac{\varphi_{ess}}{\omega_{1s}} = \frac{K_g' + 1}{K_e'} \tag{18}$$

Error-network and tachometer systems:

$$\frac{\varphi_{ess}}{\omega_{1s}} = \frac{1}{K_e'} \tag{19}$$

For a step input of torque, $T_d(s) = T_d/s$ (with $\varphi_c = \omega_{1s} = 0$), all three systems have a continuously increasing error as a function of time, since

$$\frac{\varphi_{ess}}{T_d} = \lim_{s \to 0} s\varphi_e(s) \to \infty \tag{20}$$

Although the error due to a step of T_d becomes infinite, equations for the increasing error as a function of time can be obtained by taking the inverse Laplace transform of the error equations and simplifying them for large values of time by setting all terms equal to zero which contain time as a negative exponential. The process is very straightforward, except that the third-order denominators of equations (10) and (16) must be factored or else reduced by approximation to second order if tables of Laplace transforms are to be used. Reduction of the third-order equations to second order is accomplished in the next section of this report. For the present, the approximate second-order equations are taken from the next section, and the only justification given here is that the steady-state error for torque input is dominated by the time increasing term,

which is not changed by the approximations. Specifically, for $T_d(s) = T_d/s$ with $\varphi_c = \omega_{1s} = 0$ (and $\varphi_e = -\varphi_b$), equations (42), (48), and (56) become

Rate-gyro system:

$$\varphi_e = \frac{\frac{T_d}{J_b s^2}\left(s + \frac{1}{\tau_m}\right)}{s^2 + \frac{K_g'}{\tau_m} s + \frac{K_e'}{\tau_m}}$$

Error-network system:

$$\varphi_e = \frac{\frac{T_d}{J_b s^2}\left(s + \frac{1}{\tau_m}\right)}{s^2 + \frac{K_i'}{\tau_m} s + \frac{K_e'}{\tau_m}}$$

A 4 1 8

Tachometer system:

$$\varphi_e = \frac{\frac{T_d}{J_b s^2}\left(s + \frac{1}{K_t'}\right)}{s^2 + \frac{\tau_t K_e'}{K_t'} s + \frac{K_e'}{K_t'}}$$

The resulting steady-state error equations found by taking the inverse transforms of the above equations and simplifying for large values of time are:

Rate-gyro system:

$$\frac{\varphi_{ess}}{T_d} = \frac{1}{J_b} \frac{\tau_m - \frac{K_g'}{K_e'} + t}{K_e'} \tag{21}$$

Error-network system:

$$\frac{\varphi_{ess}}{T_d} = \frac{1}{J_b} \frac{\tau_m - \frac{K_i'}{K_e'} + t}{K_e'} \tag{22}$$

Tachometer system:

$$\frac{\varphi_{ess}}{T_d} = \frac{1}{J_b} \frac{K_t' - \tau_t + t}{K_e'} \tag{23}$$

These steady-state error equations will be used in selecting system parameters as outlined in the next section.

DESIGN CRITERIA

Primary Considerations

The first step in the system design is to select tentatively the outer loop gain, the wheel angular momentum, and the motor stall torque. The outer loop gain and also the rate-gyro loop gain may be established by examining the steady-state error requirements. The angular momentum and motor stall torque may be determined if the external torque, control time, settling time, and maximum steady-state error are considered.

The first condition to be examined is the minimum outer loop gain, K_e', established by steady-state error requirements. Since K_e' must be large enough to keep the steady-state error less than or equal to its allowable maximum, equation (19) for the error-network and tachometer systems may be rewritten in the form of a requirement on K_e'

$$K_e' \geq \frac{\omega_{1s}}{\varphi_{ess_{max}}} \tag{24}$$

and equation (18) for the rate-gyro system may be rewritten as

$$K_e' \geq \frac{\omega_{1s}(K_g' + 1)}{\varphi_{ess_{max}}} \tag{25}$$

An additional requirement is placed on the outer loop gain by the error equations (21), (22), and (23) for torque input. The time for the motor amplifier to become saturated in the presence of a disturbance torque is the control time, t_c. For the Orbiting Astronomical Observatory example, t_c will be assumed to be equal to the orbital period. For such large control times, the increasing error component is dominant in equations (21), (22), and (23), yielding the following approximate equation for all three systems:

$$\frac{\varphi_{ess}}{T_d} = \frac{1}{J_b}\frac{t}{K_e'} \tag{26}$$

This equation becomes a restriction on K_e' when changed to the form

$$K_e' \geq \frac{T_d}{J_b}\frac{t_c}{\varphi_{ess_{max}}} \tag{27}$$

For the error-network and tachometer systems, both equations (24) and (27) must be tested to determine the minimum value of K_e'. For the rate-gyro system, equation (27) is used to determine the minimum value

of K_e', and equation (25) is used to determine a maximum ratio of K_g'/K_e' by rearranging the equation and simplifying for $K_g' \gg 1$ to give

$$\frac{K_g'}{K_e'} \leq \frac{\varphi_{ess_{max}}}{\omega_{1s}} \tag{28}$$

The simplifying assumption that

$$K_g' \gg 1 \tag{29}$$

is easily justified if it is noted that in equation (7) the damping term in the denominator involves $1/\tau_m + K_g'/\tau_m$, and since τ_m is large as discussed previously, most of the damping must come from the rate gyro, so that $K_g'/\tau_m \gg 1/\tau_m$.

A 4 1 8

Consideration will now be given to the angular momentum. The maximum momentum which must be stored in the wheel is equal to the disturbance torque integrated over the required control time. If the average value of T_d is used,

$$J_w\omega_{w_{max}} = T_d t_c \tag{30}$$

When equation (30) is combined with equation (27)

$$K_e' \geq \frac{J_w\omega_{w_{max}}}{J_b\varphi_{ess_{max}}} \tag{31}$$

that is, K_e' must be large enough to produce maximum motor speed without the error exceeding its permissible maximum, if all of the available momentum is to be used.

A maximum value of K_e' is set by consideration of the desired linear region of transient response for a position step input. If K_e' is made much larger than necessary, undesirable limit-cycle operation may result.

Motor stall torque will now be considered. The motor torque and corresponding settling time may be roughly estimated for large signal response if bang-bang operation is assumed, where full torque is always applied in one direction or the other. For a servomotor this means that τ_m is infinitely large. The minimum settling time results if full torque is applied in one direction until the output position has reached half of its final value and then the full torque is reversed in direction as

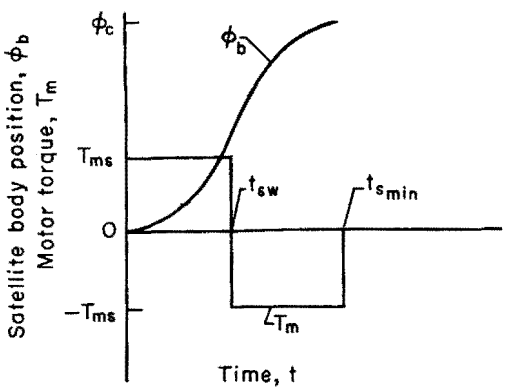

Response for bang-bang operation with minimum settling time

Sketch (e)

illustrated in sketch (e) (see ref. 2, p. 15). The minimum settling time, $t_{s_{min}}$, resulting from bang-bang operation may be derived as follows:

The known relation,

$$\varphi_b = \frac{T_m}{J_b s^2} \tag{32}$$

is used for a step input, $T_m(s) = T_{ms}/s$, to obtain

$$\varphi_b(t) = L^{-1}\frac{T_{ms}}{J_b s^3} = \frac{T_{ms}t^2}{2J_b} \tag{33}$$

A 4 1 8

or

$$t = \sqrt{\frac{2\varphi_b J_b}{T_{ms}}} \tag{34}$$

But $t = t_{sw} = t_{s_{min}}/2$ for $\varphi_b = \varphi_c/2$; therefore,

$$t_{s_{min}} = 2\sqrt{\frac{\varphi_c J_b}{T_{ms}}} \tag{35}$$

Equation (35) indicates the absolute minimum stall torque required to produce a specified settling time. In the design of practical systems there are two other considerations which must be included to estimate stall torque. First, the actual motor time constant will be somewhat less than infinity, resulting in a slightly larger torque requirement for the same settling time. The following useful equation for τ_m is derived in appendix C:

$$\tau_m = \frac{J_w \omega_{w_{max}}}{T_{ms}} \tag{36}$$

The second, and most significant, practical consideration is that compensation is generally insufficient to prevent several overshoots, and the stall torque required could well be an order of magnitude larger than would be required if no overshoots were allowed.

Generalized Linear Parameters

A study can now be made of the dynamics of the linear, or small-signal, response in order to obtain equations for the remaining system parameters, and to determine the system linear transient response.

For this linear analysis an equation must be obtained for φ_b resulting from φ_c, ω_{1s}, and T_d. If the relationship

$$\varphi_e = \varphi_c - \varphi_b + \omega_{1s}/s \tag{37}$$

obtained from sketch (b) is substituted into equations (7), (10), and (16), and the resulting equations solved for φ_b, the following equations are obtained:

Rate-gyro system:

$$\varphi_b = \frac{\left(\varphi_c + \frac{\omega_{1s}}{s}\right)\frac{K_e'}{\tau_m} - \frac{T_d}{J_b s}\left(s + \frac{1}{\tau_m}\right)}{s^2 + \left(\frac{1}{\tau_m} + \frac{K_g'}{\tau_m}\right)s + \frac{K_e'}{\tau_m}} \tag{38}$$

Error-network system:

$$\varphi_b = \frac{\left(\varphi_c + \frac{\omega_{1s}}{s}\right)\left[1 + \left(\tau_d + \frac{K_i'}{K_e'}\right)s\right]\frac{K_e'}{\tau_d\tau_m} - \frac{T_d}{J_b s}\left[s^2 + \left(\frac{1}{\tau_d} + \frac{1}{\tau_m}\right)s + \frac{1}{\tau_d\tau_m}\right]}{s^3 + \left(\frac{1}{\tau_d} + \frac{1}{\tau_m}\right)s^2 + \left(\frac{1}{\tau_d\tau_m} + \frac{K_e'}{\tau_m} + \frac{K_i'}{\tau_d\tau_m}\right)s + \frac{K_e'}{\tau_d\tau_m}} \tag{39}$$

Tachometer system:

$$\varphi_b = \frac{\left(\varphi_c + \frac{\omega_{1s}}{s}\right)\left(s + \frac{1}{\tau_t}\right)\frac{K_e'}{\tau_m} - \frac{T_d}{J_b s}\left[s^2 + \left(\frac{1}{\tau_t} + \frac{1}{\tau_m} + \frac{K_t'}{\tau_t\tau_m}\right)s + \frac{1}{\tau_t\tau_m}\right]}{s^3 + \left(\frac{1}{\tau_t} + \frac{1}{\tau_m} + \frac{K_t'}{\tau_t\tau_m}\right)s^2 + \left(\frac{1}{\tau_t\tau_m} + \frac{K_e'}{\tau_m}\right)s + \frac{K_e'}{\tau_t\tau_m}} \tag{40}$$

An analysis using generalized response parameters can now be made if the closed-loop equations can be reduced by reasonable approximations to second-order equations having the form

$$\varphi_b = \frac{\left(\varphi_c + \frac{\omega_1 s}{s}\right)\left(s + \frac{1}{\tau_1}\right)\tau_1\omega_n^2 - \frac{T_d}{J_b s}\left(s + \frac{1}{\tau_2}\right)}{s^2 + 2\zeta\omega_n s + \omega_n^2} \tag{41}$$

Equation (38) for the rate-gyro system is already in the desired form with $\tau_1 = 0$. If the assumption is made that $K_g' \gg 1$ (eq. (29)), equation (38) is simplified to

$$\varphi_b = \frac{\left(\varphi_c + \frac{\omega_1 s}{s}\right)\frac{K_e'}{\tau_m} - \frac{T_d}{J_b s}\left(s + \frac{1}{\tau_m}\right)}{s^2 + \frac{K_g'}{\tau_m}s + \frac{K_e'}{\tau_m}} \tag{42}$$

A 4 1 8

Equation (39) for the error-network system has a second-order numerator and a third-order denominator; however, the numerator and denominator may be reduced by one order each by restricting the size of the lag time constant, τ_d, to small values. If it is first assumed that

$$K_i' \gg 1 \tag{43}$$

$$\tau_m \gg \tau_d \tag{44}$$

and

$$\tau_d \ll \frac{K_i'}{K_e'} \tag{45}$$

and then the numerator and denominator of equation (39) are multiplied by τ_d, the resulting equation is

$$\varphi_b = \frac{\left(\varphi_c + \frac{\omega_1 s}{s}\right)\left(1 + \frac{K_i'}{K_e'}s\right)\frac{K_e'}{\tau_m} - \frac{T_d}{J_b s}\left(\tau_d s^2 + s + \frac{1}{\tau_m}\right)}{\tau_d s^3 + s^2 + \frac{K_i'}{\tau_m}s + \frac{K_e'}{\tau_m}} \tag{46}$$

In the numerator the term $\tau_d s^2$ may be neglected with respect to $s + 1/\tau_m$ up to frequencies somewhat above ω_n, provided $\tau_d\omega_n^2 \ll \omega_n$, or

$$\tau_d \ll \frac{1}{\omega_n} \tag{47}$$

Similarly, in the denominator, the term $\tau_d s^3$ may also be neglected, and equation (46) may be reduced to the desired form

$$\varphi_b = \frac{\left(\varphi_c + \frac{\omega_{1s}}{s}\right)\left(s + \frac{K_e'}{K_i'}\right)\frac{K_i'}{\tau_m} - \frac{T_d}{J_b s}\left(s + \frac{1}{\tau_m}\right)}{s^2 + \frac{K_i'}{\tau_m}s + \frac{K_e'}{\tau_m}} \tag{48}$$

In this equation it is seen that

$$\omega_n = \sqrt{\frac{K_e'}{\tau_m}} \tag{49}$$

A 4 1 8

and the assumption stated in equation (47) may be written as

$$\tau_d \ll \sqrt{\frac{\tau_m}{K_e'}} \tag{50}$$

The assumptions made in order to simplify the equation for the error-network system may be shown to be reasonable for most satellite control system applications. The assumption that $K_i' \gg 1$ may be justified on the same basis that $K_g' \gg 1$ is justified. The assumption that $\tau_m \gg \tau_d$ is obviously valid since the motor time constant τ_m is large, and the inherent lag time constant τ_d is desired to be small. The validity of $\tau_d \ll K_i'/K_e'$ may not be apparent from previous discussions; however, justification is readily provided by the combination of the derivative and straight-through paths for the error signal in sketch (c) for the error-rate network into a single lead-lag network with the following equation:

$$K_e' + \frac{K_i' s}{1 + \tau_d s} = \frac{K_e'\left[1 + \left(\tau_d + \frac{K_i'}{K_e'}\right)s\right]}{1 + \tau_d s} \tag{51}$$

The lag time constant must be much smaller than the lead time constant and also much smaller than the reciprocal of the natural frequency (eq. (50)) if the undesirable lag is to be insignificant during the transient response.

Equation (40) for the tachometer system also has a second-order numerator and a third-order denominator, which may be reduced by one order each by the same method used for the error-network system. If it is assumed that

$$K_e' \gg 1/\tau_t \tag{52}$$

and

$$K_t' \gg \tau_m + \tau_t \tag{53}$$

and if the numerator and denominator of equation (40) are multiplied by $\tau_t\tau_m/K_t'$, the resulting equation is

$$\varphi_b = \frac{\left(\varphi_c + \frac{\omega_1 s}{s}\right)\left(s + \frac{1}{\tau_t}\right)\frac{\tau_t K_e'}{K_t'} - \frac{T_d}{J_b s}\left(\frac{\tau_t\tau_m}{K_t'}s^2 + s + \frac{1}{K_t'}\right)}{\frac{\tau_t\tau_m}{K_t'}s^3 + s^2 + \frac{\tau_t K_e'}{K_t'}s + \frac{K_e'}{K_t'}} \tag{54}$$

In the numerator the term $(\tau_t\tau_m/K_t')s^2$ and in the denominator the term $(\tau_t\tau_m/K_t')s^3$ may be neglected provided

$$\frac{\tau_t\tau_m}{K_t'} \ll \frac{1}{\omega_n} \tag{55}$$

A4188

and equation (54) may be reduced to the desired form

$$\varphi_b = \frac{\left(\varphi_c + \frac{\omega_1 s}{s}\right)\left(s + \frac{1}{\tau_t}\right)\frac{\tau_t K_e'}{K_t'} - \frac{T_d}{J_b s}\left(s + \frac{1}{K_t'}\right)}{s^2 + \frac{\tau_t K_e'}{K_t'}s + \frac{K_e'}{K_t'}} \tag{56}$$

Here, it is seen that

$$\omega_n = \sqrt{\frac{K_e'}{K_t'}} \tag{57}$$

and the assumption stated in equation (55) may be written as

$$\frac{\tau_t\tau_m}{K_t'} \ll \sqrt{\frac{K_t'}{K_e'}} \tag{58}$$

The assumptions made to obtain the simplified equation for the tachometer system are not quite as general as the ones made for the error-network system, and no attempt will be made to justify them. However, for any case in question, after values for the various parameters have been selected, the simplifying assumptions may be easily tested to see whether the simplification was justified.

Equations (42), (48), and (56) have the form of equation (41) so it is a simple matter now to solve for the generalized linear parameters, ω_n, ζ, $1/\tau_1\omega_n$, and $1/\tau_2\omega_n$, for the three systems. The results, including the assumptions used for simplifying the closed-loop equations, are listed in table I. The quantities $1/\tau_1\omega_n$ and $1/\tau_2\omega_n$ are used instead of $1/\tau_1$ and $1/\tau_2$ because the response is affected by the size of $1/\tau_1$ and $1/\tau_2$ relative to ω_n.

The choice of the best numerical values for the generalized linear parameters is based mostly upon the following three considerations: (1) ζ should be greater than 0.3 and less than 1.0 for good stability without sluggishness, (2) $1/\tau_1$ should be nearly equal to or greater than ω_n so that the response for an initial displacement is not greatly affected by the position zero, $1/\tau_1$, which tends to make the response highly oscillatory, and (3) ω_n should be large enough for fast response. It should be mentioned here that the torque zero has a value $1/\tau_2 \ll \omega_n$ for all practical cases. Hence, at the high frequencies of concern for transient response, where $\omega > \omega_n$, the term $s + 1/\tau_2$ reduces to s, and the numerator term associated with torque becomes T_d/J_b. Torque inputs are small and change only gradually, and therefore, they have little effect on the transient response.

A
4
1
8

Numerical Example of Design Procedure

The design criteria which have been established can now be applied to the numerical example of the Orbiting Astronomical Observatory (OAO). From the most stringent fine control requirements presently contemplated for the OAO, the following specifications for stellar sighting have been assumed:

Maximum steady-state error: $\varphi_{essmax} = 0.1$ second of arc

Maximum initial error: $\varphi_{eo} = 60$ seconds of arc

Approximate settling time: $t_s \cong 1$ minute

Control time: $t_c = 105$ minutes $= 6300$ seconds

Maximum line-of-sight velocity: $\omega_{ls} = 0.01$ second of arc/second

Maximum roll (about line of sight) velocity: $\omega_r = 1.0$ second of arc/second

Maximum disturbance torque: $T_d = 100$ dyne cm

Body inertia: $J_b = 10^{10}$ gram cm^2

These specifications will now be applied to the selection of numerical values for all three systems. The outer loop gain, wheel angular momentum, and motor stall torque will be determined first. The outer loop gain must be large enough to satisfy equation (24) for ω_{ls} input and equation (27) for T_d input. For the OAO the gain requirement of equation (27) is much larger, and the resulting value for $t_c = 6300$ seconds is

$$K_e' \geq 130 \text{ (radians/sec)/radian} \tag{59}$$

A value of K_e' with a slight margin of safety is now chosen as $K_e' = 150$ (radians/second)/radian.

The required angular momentum capacity is readily obtained from equation (30). When values for the OAO are substituted,

$$J_w \omega_{w_{max}} = 6.3(10)^5 \text{ gram cm}^2/\text{sec} \tag{60}$$

If the servomotor has a maximum speed of $\omega_{w_{max}} = 6{,}000$ rpm then the wheel inertia is $J_w = 10^3$ gram cm^2. A 4 1 8

To determine motor stall torque (and the corresponding motor time constant), equations (35) and (36) are plotted in figure 1. The solid line, representing equation (35), shows that for a minimum settling time of 60 seconds, the motor stall torque must be at least $3.3(10)^3$ dyne cm. For this stall torque the motor time constant from equation (36) is 190 seconds, which is large enough to produce nearly the same response as a τ_m of infinity. It should be emphasized that the motor stall torque given by equation (35) is for minimum settling time with no overshoots. As will be verified later in the section on large-signal analysis, the actual stall torque required is nearly an order of magnitude larger than the minimum. For the present, a value of T_{ms} is somewhat arbitrarily chosen as $T_{ms} = 2.1 \times 10^4$ dyne cm $\cong$ 0.3 oz in. The corresponding value of motor time constant is $\tau_m = 30$ seconds. This value of motor time constant is still large enough to have a relatively small effect upon the required motor stall torque as compared with the large effect of the overshoots in the response.

Consideration will now be given to the linear design parameters, ζ, $1/\tau_1$, and ω_n. Using the first row of table I, it is seen that for the rate-gyro case, there is no zero at $1/\tau_1$. For the error-network and tachometer systems, it can be observed from table I that the following convenient relationship exists:

$$\zeta = \frac{\tau_1 \omega_n}{2} \tag{61}$$

That several reasonable solutions exist for the error-network and tachometer systems is demonstrated by selecting values of ζ, such as 0.5 and 0.7, and calculating the corresponding values of $1/\tau_1\omega_n$, which are 1.0 and 0.7, respectively. From figure 1.21 in reference 3 the resulting percentages of overshoot are found to be 30 percent for $\zeta = 0.5$ and 20 percent for $\zeta = 0.7$. In the case of the rate-gyro system, where no position zero is present, the percentages of overshoot for $\zeta = 0.5$ and 0.7 are 16 and 5 percent, respectively.

A damping ratio of $\zeta = 0.7$ will now be selected for all three systems, with the corresponding position zeros for the error-network and tachometer systems located at $1/\tau_1\omega_n = 0.7$. From formulas for damping ratio in table I and the values of τ_m and K_e' previously selected, the following are calculated:

$$\frac{\tau_t}{\sqrt{K_t'}} = \frac{2\zeta}{\sqrt{K_e'}} = 0.114 \text{ sec}^{1/2} \tag{62}$$

and

$$\frac{K_g'}{K_e'} \text{ or } \frac{K_i'}{K_e'} = 2\zeta\sqrt{\frac{\tau_m}{K_e'}} = 0.625 \text{ radian/(radian/sec)} \tag{63}$$

When the above value of K_g'/K_e' is compared with the error requirement of equation (28), it is found that 0.625 is satisfactory since it is considerably less than the maximum allowable value of 10.

Since K_e' has already been selected, K_g' and K_i' may be determined from equation (63), which gives K_g' or $K_i' = 94$ radians/radian. For the tachometer system, however, τ_t and K_t' in equation (62) are not yet determined, since their selection is dependent upon the natural frequency, which will now be examined.

For the rate-gyro and error-network systems, the natural frequency calculated from table I is $\omega_n = 2.24$ radians/second which seems reasonable for a settling time of one minute. If it were necessary, ω_n could be altered by changing either τ_m or K_e', except that K_e' must remain larger than the minimum given in equation (59). If a natural frequency of 2.24 radians/second is used for the tachometer system, the resulting tachometer loop gain calculated from an expression in table I is $K_t' = 30$ radians/(radian/second), and the value of τ_t calculated from equation (62) is $\tau_t = 0.625$ second. These values for K_t' and τ_t must be held in abeyance until the simplifying assumptions are checked.

Before the simplifying assumptions for the three systems are checked, a value should be selected for τ_d, which is the only remaining parameter to be chosen. The only demands on τ_d are that it be small enough to satisfy the assumptions and prevent excessive delays, but large enough to be realizable. It would seem reasonable for a physical network that the lead time constant be at least ten times the size of the lag time constant. A value of $\tau_d = 0.01$ second will be selected, which is slightly over 60 times smaller than K_i'/K_e'. It will be shown later that the value of τ_d can change over a wide range without significantly affecting the response.

When all the values which have been chosen are substituted into the expressions in table I, the results shown in table II are obtained for the rate-gyro and error-network systems and Case A of the tachometer system.

(Case B will be discussed later.) A check of the simplifying assumptions shows that all of them are satisfied for the rate-gyro and error-network systems. For the tachometer system, however, equations (53) and (58) are not satisfied. Hence, equation (56) for the tachometer system is not valid when using the values chosen thus far. Further examination of the exact closed-loop equation is required to predict the response. Obtaining an exact solution is difficult because of the third-order denominator, and further analysis of this problem will be delayed until the large-signal response has been considered.

LARGE-SIGNAL RESPONSE

The linear analysis just completed is satisfactory for relatively small angular errors. However, for many satellites, the desired range of the attitude control system will be extremely large. In the particular case of the OAO the control system may have an initial error of up to 60 seconds of arc, and still the system must control the vehicle attitude to within 0.1 second of arc. The criteria which have been used in the selection of K_e' imply that an error greater than 0.1 second of arc saturates the motor amplifier. Accordingly, a nonlinear analysis of system operation must be undertaken.

A418

Nonlinear Analysis

The parameters which have been selected by the linear analysis for small-signal response, will now be used in a nonlinear analysis to obtain the settling time in a more exact fashion than the bang-bang study made earlier (eq. (35)). The large-signal settling time will be obtained, and methods for reducing this settling time to a minimum will be considered. A semigraphical approach called the "switching time" method, presented in reference 2, is well adapted to this problem.

In order to apply the method, the block diagram for the three systems is first redrawn from sketches (b), (c), and (d) into the form shown in sketch (f). The velocity and torque inputs are omitted from the sketch;

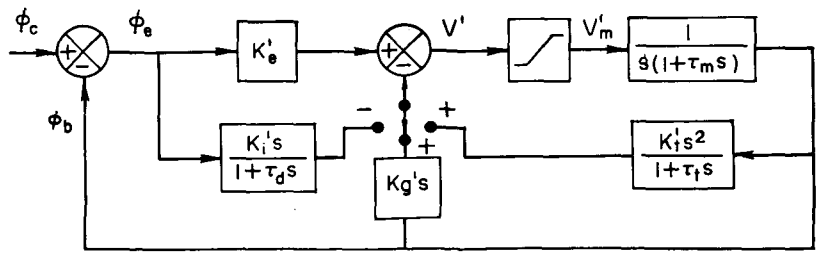

Block diagram using loop gains and selector switch

Sketch (f)

the loop gains are treated as single terms; the motor, wheel, and body are combined into a type[1] one, second-order plant; and a switch is included to select the method of damping. The plant is immediately preceded by a box representing amplifier saturation where the level of saturation is given by the fictitious voltage, $V_{m'_{max}}$, which is defined as

$$V_{m'_{max}} = K_m V_{m_{max}} \frac{J_w}{J_b} = \omega_{w_{max}} \frac{J_w}{J_b} \tag{64}$$

For the systems shown in sketch (f), the following equations relating t_{sw} to $t_{\Delta\varphi_e}$ and $\Delta\varphi_e$ (where $t_{\Delta\varphi_e}$ is the time for the error to change from one point of zero velocity to the next, and $\Delta\varphi_e$ is the incremental error change during $t_{\Delta\varphi_e}$) are derived in reference 2 (eqs. (70) and (72)):

A 4 1 8

$$\Delta\varphi_e = V_{m'_{max}} \left(2t_{sw} - t_{\Delta\varphi_e} \right) \tag{65}$$

$$t_{\Delta\varphi_e} = \tau_m \ln \left(2e^{\frac{t_{sw}}{\tau_m}} - 1 \right) \tag{66}$$

For these equations and the accompanying analysis to be valid, it is required that $V_{m'_{max}} \ll K_e' \Delta\varphi_e$, so that the error signal saturates the amplifier most of the time. It is assumed that the duration of linear operation is negligible and that the reversal of full motor voltage occurs instantaneously as V' passes through zero. It is also assumed that the initial velocity (of the wheel or satellite) is zero; in many instances the initial velocity will be zero, and furthermore, analog computer results will be presented later to show that large initial velocities do not affect the general conclusions.

The previous two equations can be solved simultaneously, and curves of t_{sw} and $t_{\Delta\varphi_e}$ versus $\Delta\varphi_e$ can be plotted, using the value of $V_{m'_{max}}$ for a particular system. For illustration the previous numerical example will be used. By substituting values which have already been chosen into equation (64), it is found that $V_{m'_{max}} = 6.3(10)^{-5}$ radians/second for all three systems. When this value for $V_{m'_{max}}$ and $\tau_m = 30$ seconds are used in equations (65) and (66), the solid-line curves of figure 2 are obtained.

---

[1]In this report "type" is used to refer to the number of integrations of the plant, or the number of poles at the origin (ref. 2, p. 7).

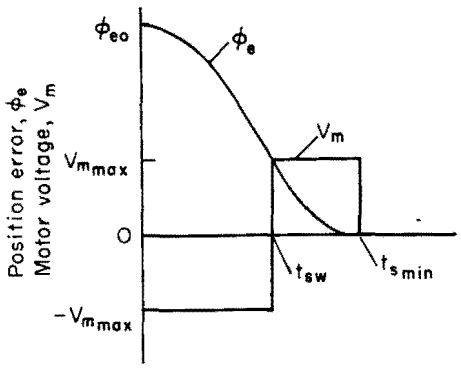

Response for minimum settling time

Sketch (g)

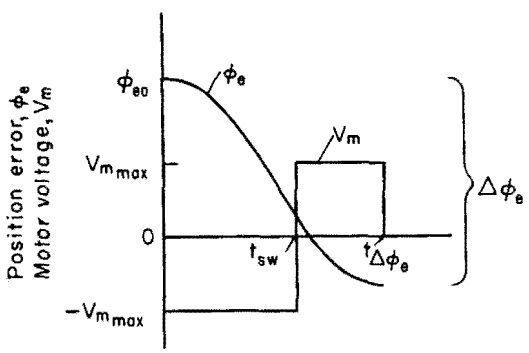

Half cycle of response for $\phi_{eo} \neq \Delta\phi_e$

Sketch (h)

The usual application of these curves is illustrated in sketch (g), which is very similar to sketch (e). For $\varphi_{eo} = \Delta\varphi_e$, the reversal of V' in sketch (f) at t_{sw} causes the system to reach a condition of zero velocity and zero position simultaneously at $t_{\Delta\varphi_e} = t_{s_{min}}$. Since there is no overshoot, there will be no further motion of the system output. For the large-signal analysis, it will be convenient to use the curves of t_{sw} and $t_{\Delta\varphi_e}$ in a slightly different fashion, as illustrated in sketch (h). Here, $\varphi_{eo} \neq \Delta\varphi_e$, and the error does not reach a condition of zero velocity and zero position simultaneously. However, since the motor voltage is reversed at the same time as in sketch (g), the two curves still have the same shape. For known values of t_{sw} and φ_{eo}, the time for one-half cycle of operation is determined as $t_{\Delta\varphi_e}$, and the magnitude of the overshoot is determined as $\Delta\varphi_e$ minus φ_{eo}. The overshoot in sketch (h) may be treated as the starting point for determining another half-cycle of operation.

A 4 1 8

For the large-signal analysis, the rate-gyro system will be considered first. The relationship between t_{sw} and φ_{eo} may be obtained by writing an equation for V' in sketch (f). From the time of initial displacement until the first reversal time, the equation for V' for the rate-gyro system for a step input $\varphi_c(s) = \varphi_{eo}/s$ (and the corresponding $V_m'(s) = V_{m'_{max}}/s$) is

$$V' = \frac{\varphi_{eo}}{s} K_e' - \frac{V_{m'_{max}}}{s^2}\left(\frac{K_e' + K_g' s}{1 + \tau_m s}\right) \qquad (67)$$

Taking the inverse Laplace transform, dividing by K_e', and rearranging, we obtain

$$\frac{V'}{K_e'} - \varphi_{eo} = \tau_m V_{m_{max}}' \left[\left(\frac{\tau_m - \frac{K_g'}{K_e'}}{\tau_m} \right) \left(1 - e^{-\frac{t}{\tau_m}} \right) - \frac{t}{\tau_m} \right] \tag{68}$$

Setting $V' = 0$ for $t = t_{sw}$, and replacing $(\tau_m - K_g'/K_e')/\tau_m$ by the letter C, changes the equation into the approximate relation

$$\varphi_{eo} = \tau_m V_{m_{max}}' \left[\frac{t_{sw}}{\tau_m} - C \left(1 - e^{-\frac{t_{sw}}{\tau_m}} \right) \right] \tag{69}$$

A 4 1 8

This equation is used to determine a curve of t_{sw} versus φ_{eo} in figure 2, using a value for $C = 0.979$, which corresponds to the previously selected values of $\tau_m = 30$ seconds and $K_g'/K_e' = 0.625$ radian/(radian/second). If now an initial error angle of $\varphi_{eo} = 60$ seconds of arc is assumed, then from the curve of t_{sw} versus φ_{eo} it is seen that $t_{sw} = 17.7$ seconds. The corresponding value of $\Delta\varphi_e$ from the curve of t_{sw} versus $\Delta\varphi_e$ is 86.4 seconds of arc, and the value of $t_{\Delta\varphi_e}$ from the curve of $t_{\Delta\varphi_e}$ versus $\Delta\varphi_e$ is 28.8 seconds. As illustrated in figure 3, the total angular change of 86.4 seconds of arc produces an overshoot of 26.4 seconds of arc, and hence, the input for the next half cycle of the oscillation is 26.4 seconds of arc. Using $\varphi_{eo} = 26.4$ seconds of arc in figure 2 gives $t_{sw} = 11.2$ seconds, which results in $t_{\Delta\varphi_e} = 19.2$ seconds. The corresponding overshoot is found to be 10.1 seconds of arc. The process can be continued to as small an overshoot as desired, and the settling time is found by adding the times for the successive half-cycles of oscillation. For the example being considered, the settling time from $\varphi_e = 60$ seconds of arc to 0.1 second of arc is about 83 seconds as illustrated in figure 3. This value becomes one point on a curve of t_s versus φ_{eo} in figure 2 (where outer scale is used for t_s). Repeating this process for different initial errors gives values for the entire curve for t_s. In figure 3 the motor drive voltage has been sketched to show the points at which switching occurs.

It is interesting to note for comparison with sketch (e) that in sketch (g), which was obtained from figure 2, t_{sw} is somewhat longer than one-half $t_{s_{min}}$. This actually indicates that a higher torque is applied during the deceleration period than during the acceleration period. The explanation for this is that the motor speed is increasing until t_{sw}; as

a result, the reversal torque is larger than the stall torque as illustrated by the broken line in sketch (i), whereas for sketch (e) the torque is independent of wheel speed.

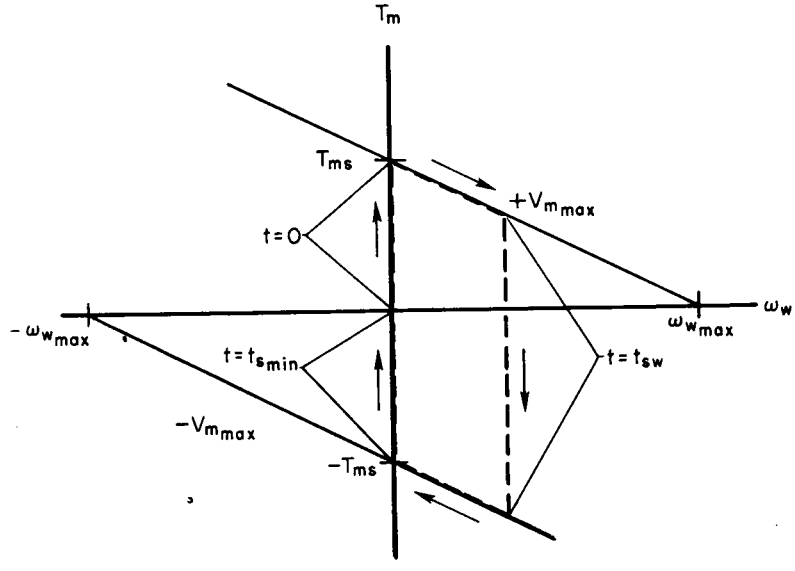

Motor torque–speed curve

Sketch (i)

The switching-time method can also be used to determine an optimum nonlinear relationship between gain and error signal which will reduce t_s to $t_{\Delta\varphi_e} = t_{s_{min}}$ (with no overshoots). The process will be illustrated for the rate-gyro system. The first step is to solve for K_e' in equation (68) with $V' = 0$ for $t = t_{sw}$.

$$K_e' = \frac{\frac{K_g'}{\tau_m}\left(1 - e^{-\frac{t_{sw}}{\tau_m}}\right)}{\frac{\varphi_{eo}}{\tau_m \omega_{w'_{max}}} + 1 - e^{-\frac{t_{sw}}{\tau_m}} - \frac{t_{sw}}{\tau_m}} \qquad (70)$$

The next step is to identify the error signal by first writing the Laplace transform equation from sketch (f) for a step input.

$$\varphi_e = \frac{\varphi_{eo}}{s} - \frac{V_{m'max}}{s^2(1 + \tau_m s)} \tag{71}$$

Then taking the inverse transform and replacing t by t_{sw} produces

$$\varphi_e\Big]_{t_{sw}} = \tau_m V_{m'max} \left(\frac{\varphi_{eo}}{\tau_m V_{m'max}} + 1 - e^{-\frac{t_{sw}}{\tau_m}} - \frac{t_{sw}}{\tau_m} \right) \tag{72}$$

A comparison of the above equation with the denominator of equation (70) shows that

$$K_e' = \frac{K_g' V_{m'max} \left(1 - e^{-\frac{t_{sw}}{\tau_m}} \right)}{\varphi_e\Big]_{t_{sw}}} \tag{73}$$

In the above derivation K_e' was considered to be a constant; however, since the system is always limited except at the switching point, the value of K_e' is of no significance (as long as it is sufficient to cause saturation) except at t_{sw}. Hence, equation (73) may equally well be considered as defining K_e' in terms of instantaneous error, φ_e, instead of $\varphi_e]_{t_{sw}}$, since K_e' will then always have the desired value at t_{sw}. In order to prevent overshoots the desired relationship between t_{sw} and φ_{eo} may be obtained from the curve of t_{sw} versus $\Delta\varphi_e$ with $\varphi_{eo} = \Delta\varphi_e$.

For the numerical example being considered, $K_g' = 94$ radians/radian and $\tau_m = 30$ seconds, giving a value for K_g'/τ_m of 3.13 (radians/second)/radian. To illustrate how one point on the nonlinear curve of optimum gain versus error is obtained, a t_{sw} of 13.5 seconds is arbitrarily chosen, and the corresponding input is read from the curve of t_{sw} versus $\Delta\varphi_e$ in figure 2 as $\varphi_{eo} = \Delta\varphi_e = 55$ seconds of arc. Equation (70) is then solved for K_e', which is found to be 21.4 (radians/second)/radian, and equation (72) is solved for $\varphi_e]_{t_{sw}}$, which is found to be 20.7 seconds of arc. These values are used to plot one point on the curve of optimum gain in figure 4(a) (where $\varphi_e]_{t_{sw}}$ has been replaced by φ_e as previously justified), which shows the relationship between outer loop gain and instantaneous position error required to produce minimum settling time for any initial error.

The actual output-input relationship of the error amplifier producing K_e' is shown in figure 4(b), where the ordinate is found by merely multiplying K_e' by φ_e from figure 4(a). The constant gain prescribed by the previous linear analysis is illustrated in figure 4 by straight lines. It

should be mentioned that an optimum relation between K_g' and φ_e to produce minimum settling time with constant K_e' could be calculated in the same manner. For the rate-gyro system the nonlinearity in K_e' required for optimum switching to produce minimum settling time may conveniently be considered to represent a nonlinear sensor gain K_s, since K_g' does not include K_s and therefore the rate damping is not affected by sensor gain.

The error-network system will now be analyzed for large-signal response in the same manner as the rate-gyro system. The Laplace transform equation for V' from sketch (f) for a step input is

$$V' = \left[\frac{\varphi_{eo}}{s} - \frac{V_{m_{max}}'}{s^2(1 + \tau_m s)}\right]\left(K_e' + \frac{K_i' s}{1 + \tau_d s}\right) \tag{74}$$

A 4 1 8

Taking the inverse transform, dividing by K_e', and rearranging gives

$$\frac{V'}{K_e'} - \varphi_{eo}\left(1 + \frac{K_i'}{\tau_d K_e'} e^{-\frac{t}{\tau_d}}\right) = \tau_m V_{m_{max}}'\left[\left(\frac{\tau_m - \tau_d - \frac{K_i'}{K_e'}}{\tau_m - \tau_d}\right)\left(1 - e^{-\frac{t}{\tau_m}}\right)\right.$$

$$\left. + \left(\frac{\tau_d K_i'}{\tau_m K_e'}\right)\left(\frac{1 - e^{-\frac{t}{\tau_d}}}{\tau_m - \tau_d}\right) - \frac{t}{\tau_m}\right] \tag{75}$$

Letting $V' = 0$ for $t = t_{sw}$, assuming $\tau_d \ll \tau_m$, and replacing $(\tau_m - K_i'/K_e')/\tau_m$ by C changes the equation into the approximate relation

$$\varphi_{eo} = \tau_m V_{m_{max}}'\left[\frac{t_{sw}}{\tau_m} - C\left(1 - e^{-\frac{t_{sw}}{\tau_m}}\right)\right] \tag{76}$$

which is identical to equation (69) for the rate gyro. Hence, the same curves may be applied, as shown in figures 2, 3, and 4, except that K_i' is used instead of K_g'. It should be noted that unlike the rate-gyro system, the nonlinear gain in figure 4 cannot be applied to the sensor for the error-network system, since K_i' also includes K_s and the rate damping is affected by sensor gain.

For the tachometer system, the equation for V' is

$$V' = \frac{\varphi_{eo}}{s} K_e' - \frac{V_{m_{max}}'}{s^2}\left(\frac{K_e' + \frac{K_t' s^2}{1 + \tau_t s}}{1 + \tau_m s}\right) \tag{77}$$

Taking the inverse transform and dividing by K_e',

$$\frac{V'}{K_e'} - \varphi_{eo} = \tau_m V_{m_{max}}'\left[1 - e^{-\frac{t}{\tau_m}} - \left(\frac{K_t'}{\tau_m K_e'}\right)\left(\frac{e^{-\frac{t}{\tau_m}} - e^{-\frac{t}{\tau_t}}}{\tau_m - \tau_t}\right) - \frac{t}{\tau_m}\right] \tag{78}$$

Letting $V' = 0$ for $t = t_{sw}$,

$$\varphi_{eo} = \tau_m V_{m_{max}}'\left[\left(\frac{K_t'}{\tau_m K_e'}\right)\left(\frac{e^{-\frac{t_{sw}}{\tau_m}} - e^{-\frac{t_{sw}}{\tau_t}}}{\tau_m - \tau_t}\right) - 1 + e^{-\frac{t_{sw}}{\tau_m}} + \frac{t_{sw}}{\tau_m}\right] \tag{79}$$

Switching- and settling-time curves for the tachometer system are shown in figure 5. For case A, $\Delta\varphi_e$ is significantly larger than φ_{eo} for small inputs. The resulting oscillatory response and long settling time are illustrated in figure 6, which was obtained by the same graphical procedure described previously for the rate-gyro system. When the tachometer-loop gain, K_t', is increased by a factor of 100 and the damping ratio is kept nearly the same by increasing τ_t to 5 seconds, as shown in case B of table II, then the large-signal response becomes much more reasonable as shown in figure 6. It should also be observed that for case B in table II, the simplifying assumptions are satisfied. For the graphical computation of settling time in figure 5, t_s was assumed to be approximately equal to $t_{\Delta\varphi_e}$ for $\varphi_{eo} < 13$ seconds of arc, because the method of reference 2 applies only for $\Delta\varphi_e > \varphi_{eo}$. However, the approximation is reasonably valid in figure 5 because it is used for only a small portion of the settling time. In passing, it should be mentioned that the increased value of K_t' can no longer be completely neglected in equation (23) for the steady-state error due to T_d.

Obtaining the optimum gain requirements for reducing the settling time to a minimum for the tachometer system involves certain restrictions outlined in reference 2 and will not be attempted here.

Analog Computer Results

In order to provide a check of the analyses previously presented, studies of wheel control systems were carried out on an analog computer. Using the same numerical example, small-signal simulation of the exact systems (third-order equations) verified the response predicted by the approximate linear analysis. In the presence of 100 dyne cm of external torque and a small initial displacement, all three systems tracked to within 0.1 second of arc for 105 minutes with a dynamic response and error buildup that agreed very well with that predicted by the second-order equations using generalized linear parameters. Only large-signal data will be discussed here because the linear response is well defined by generalized second-order curves. For the large-signal computer analysis the block diagrams of sketches (b), (c), and (d) were converted to the computer circuit shown in figure 7.

The sensor output was limited at the values of φ_{e1} shown in figure 8. It is interesting to note that a limited sensor output results in a nonlinear sensor gain which is similar to the optimum gain shown in figure 4. Although the largest value of error limiting used was $\varphi_{e1} = 10$ seconds of arc, it was shown that very little change in response would have resulted from further increases in the size of the limit.

Transient response curves for the three systems, using the parameters selected in the previous linear and nonlinear analyses, are presented in figures 9 and 10. These curves represent large-signal response, and they correspond very well with the predictions made in figures 3 and 6. Graphs showing the effect of error limit on settling time are shown for the three systems in figures 11, 12, and 13. From the figures it is apparent that settling time is essentially independent of the linear sensor range for all three systems for $\varphi_{e1} > 6$ seconds of arc. Some comparison can be made between figures 11, 12, and 13 from the analog computer and figures 2 and 5 from the large-signal analysis. For the rate-gyro and error-network systems, the computer settling time of 85 seconds agrees quite well with the 83 seconds calculated settling time from figure 2. For the tachometer system (case B) the computer settling time of 75 seconds is somewhat larger than the calculated value of about 60 seconds from figure 5, due to the approximation of t_s by $t_{\Delta\varphi_e}$ for $\varphi_{eo} < 13$ seconds of arc in the calculations.

The dip in the settling-time curves for the rate-gyro case of figure 11 apparently results from the curves of figure 8 approaching the optimum curves of figure 4, thus the overshoot is reduced so that the settling time approaches $t_{\Delta\varphi_e}$. It should be observed, however, that the dips in the curves of figure 11 still remain somewhat above the minimum value for settling time of $t_{s_{min}} = t_{\Delta\varphi_e} = 24$ seconds shown in figure 2 for $\Delta\varphi_e = 60$ seconds of arc. For small error limits, the settling-time curve for the error-network system shown in figure 12 does not have a dip like that of the rate-gyro system, because the damping of the error-network system is reduced by limiting the error signal. For the tachometer

system there is a significant increase in settling time for small error limits as shown in figure 13, which can be explained from figure 5. For small effective values of φ_{eo} produced by small φ_{e1}, φ_{eo} is greater than $\Delta\varphi_e$ for a significant portion of the settling time, resulting in overdamped operation and long settling times.

The effects on settling time of the time constants of the error-rate and tachometer networks are shown in figures 14 and 15. For the error-network system, t_s is nearly independent of τ_d for $\tau_d < 1.0$ second. For the tachometer system, however, there is a broad minimum. When adjusting τ_t to obtain this minimum, it must be remembered that the damping ratio for the linear region is directly proportional to the tachometer network time constant, τ_t.

A
4
1
8

The graph in figure 16 of settling time versus motor time constant obtained from the computer results for the rate-gyro and error-network systems shows an approximately linear relationship. For the particular parameters selected, the settling time is about three times the motor time constant.

The effect of initial wheel velocity on transient response is shown in figure 17 for the rate-gyro and error-network systems. Comparison of the curves shows that an initial wheel speed of one-half the maximum decreases the overshoot and settling time somewhat when applied in one direction, but increases the overshoot and settling time when applied in the other direction. Computer results were also obtained to show that initial body velocities of $\pm(1/2)\omega_{w_{max}}J_w/J_b = \pm 3.15\times10^{-5}$ radians/second had similar effects on the shape of the response curve and lengthened the settling time to about 120 seconds.

THREE-DIMENSIONAL PROBLEMS

General Considerations

Speculation about three-dimensional control points to at least two causes of unwanted cross-coupling torques. One of the most obvious causes is the change in direction of the angular momentum vector of a gyro or inertia wheel, which is well understood as a means of producing a torque about an output axis which is perpendicular to the input axis. Another apparent cause of cross-coupling torques is the misalinement of the wheel axes with the principal body axes, or the addition of an unbalancing mass between the axes of an otherwise balanced system, which results in products of inertia being present in the body. Both of these causes were considered on the analog computer for the numerical example being considered; however, before the results are described, some mention should be made of the angular momentum transfers required for satellite fine-control systems.

For a stellar-pointing satellite, such as the OAO, any initial angular momentum of the body is absorbed into the wheels, and only small changes of wheel angular momentum are then required to overcome external disturbance effects. For an earth-pointing satellite any initial angular momentum of the body is absorbed into the wheels in the same manner as for a stellar-pointing satellite; however, large exchanges of angular momentum are required between the two wheels whose axes are in the orbital plane to maintain the total angular momentum constant as the satellite rotates in orbit. Thus the speed of two of the wheels will have an undamped oscillation at the orbital frequency. In general the control system response is relatively rapid, and the oscillation can be considered to be quasi-steady state. Three-dimensional design and simulation for an earth-pointing satellite, then, can be handled the same as for a stellar-pointing satellite by using a larger and slowly changing velocity input (ω_{1s}).

Analog Computer Results

Some analog computer results were obtained to study the theoretical three-dimensional behavior of the numerical example. The response was examined both with and without products of inertia for a system using three inertia wheels with mutually orthogonal axes. Tight control was maintained about the two axes which were perpendicular to the line of sight, and an undamped sinusoidal velocity was allowed about the line-of-sight axis with a maximum of $\omega_r = 50$ seconds of arc/second, which is 50 times the value given in the specifications for the OAO example.

The cross-coupling terms due to the directional changes of wheel and gyro momentum vectors were found to be relatively insignificant. Furthermore, when inertia unbalance ranging from 1 to 5 percent of the body inertia was placed between the axes (to produce products of inertia), its effect on the dynamic short-term response was negligible. When the roll rate of 50 seconds of arc/second was combined with near maximum wheel speed of several thousand rpm, the error exceeded the allowable maximum after several minutes. At the normal roll rate of 1 second of arc/second, however, the control time would not seriously be reduced below its estimated value of 105 minutes.

EXPERIMENTAL TESTING

Description of Apparatus

To verify the calculations for design and to investigate the physical problems to be encountered, an experimental apparatus was assembled. Control systems were mounted on a low-friction, three-degree-of-freedom platform, and control was maintain about the pitch and yaw axes, while the

platform was allowed to drift slowly about the roll axis. Data for the error-network system will be presented here, and some comment will be made about results obtained for a rate-gyro system which was also tested. The tachometer system was not tested because of the unavailability of any sort of tachometer device having the wide dynamic range demanded. A suitable device would have to be able to sense changes in speed of a fraction of an rpm while the wheel is turning at several thousand rpm.

The main piece of test equipment for obtaining experimental data was a platform supported on an air bearing (fig. 18). The actual air bearing, which is obscured in this picture by the platform, consists of a finely machined ball mounted in a cup with air injected from the bottom at about 40 psig. The air bearing provides a low-friction support to simulate frictionless space conditions, and the 6-foot-diameter platform simulates the inertial mass of the body and provides an attachment surface for control-system instruments. An angular error detector was desired which would produce an output error signal essentially equivalent to that of a star tracker; that is, a device whose output was sensitive to angular errors of fractions of a second of arc and linear over a region of many seconds of arc. The device selected is shown in sketch (j), including the light source and light sensor. Although this light source was uncollimated and has spectral characteristics, different from that of a star, it was adequate for this study. The output from the light source is obtained by using a ball bearing in a black box to reflect light which has been focused by a lens and filtered through a hole. Direct current lamp excitation is used to maintain constant light intensity.

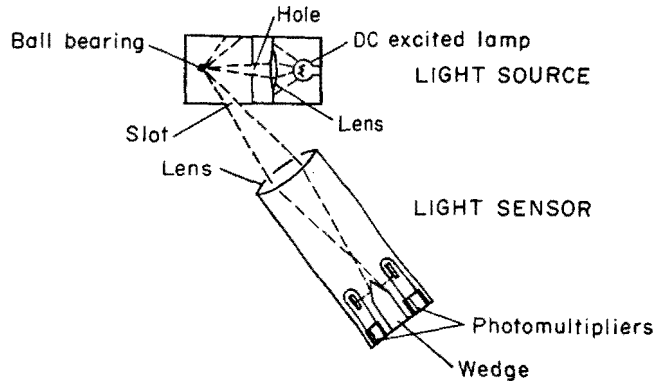

Light source and light sensor

Sketch (j)

The light from the light source is focused onto a wedge for one-dimensional control, which splits the light between two photomultipliers. An error signal is obtained by connecting the outputs of the

photomultipliers to a differential amplifer. For two-dimensional control, the wedge is replaced by a four-sided pyramid and two additional photomultipliers are used. The region of linear sensor operation is determined by the spot size on the pyramid, since the voltage output is constant when all of the spot is focused onto one pyramid face.

The d-c error output from the sensor (i.e., from the differential amplifier) was modulated before it was amplified by a-c amplifiers, which were used to minimize drift. Since a-c lead networks posed operational problems, the lead signal for the error-network system was obtained by demodulating, d-c shaping, and remodulating. The motors used to drive the inertia wheels were a-c servomotors.

Inputs and Parameters

After pendulosity torques were minimized by shifting vertical weights and the platform was finely balanced (within 1,000 dyne cm) by shifting horizontal weights, the disturbance torques were measured. The three most important torque inputs were the air-bearing turbine torque, the air-mass-circulation torque, and the building-vibration torque. Magnetic torques, which were already very small, were minimized by constructing the platform from nonmagnetic materials. The turbine torque, which acted about the yaw axis, was due to imperfect air flow in the bearing seat, and seemed to be relatively constant at nearly 10,000 dyne cm in the counterclockwise direction. Random air mass circulation and building vibration torques produced peak inputs on the order of 10,000 dyne cm, acting predominantly about the pitch and roll axes. Position error inputs up to roughly 60 seconds of arc were obtained by blowing gently on the platform.

It should be mentioned that position measurements which were taken with the sensor previously described[2] were accurate only in a dynamic sense, since the sensor was used to measure accurately position relative to its null signal position, and no attempt was made to minimize slow drifts in the sensor in order to measure absolute pointing position relative to the actual direction of the light source.

The parameters used for the error-network system may now be presented. The platform inertia had a value of $J_b = 3\times10^8$ gram cm^2, and the wheel inertia had a value of $J_w = 7.8\times10^3$ gram cm^2. The servomotor and inertia wheel combination had the following characteristics: $T_{ms} = 0.6$ in. oz, $V_{m_{max}} = 40$ volts, $\tau_m = 100$ seconds, and $\omega_{w_{max}} = 560$ radians/second. The resulting motor gain was $K_m = \omega_{w_{max}}/V_{m_{max}} = 14$ (radians/second)/volt. Since the external torque inputs were high, the motor amplifier was made to saturate for an error of 10 seconds of arc instead of 0.1 second of arc, The specific gains used were $K_s = 1.2\times10^2$ volts/radian, $K_e = 6.7$ volts/volt, and $K_a = 100$ volts/volt. Using these values the outer loop

[2]These measurements were also verified with a precision autocollimator.

gain was found to be $K_e' = 290$ (radians/second)/radian. A damping ratio of $\zeta = 0.7$ was selected, which required that the error-network loop gain have a value of $K_i' = 240$ radians/radian, or $K_i = 550$ volts/(volt/second).

The parameters which were selected can be used to predict the small-signal and large-signal responses. As mentioned previously, a damping ratio of $\zeta = 0.7$ results in a position zero at $1/\tau_1\omega_n = 0.7$ and a corresponding overshoot of 20 percent. From the expressions in table I, the natural frequency is found to be $\omega_n = 1.7$ radians/second, and the zero for torque input is found to be $1/\tau_2\omega_n = 0.0061$. A response curve obtained on the analog computer for a small-signal initial error of $\varphi_{eo} = 10$ seconds of arc is shown in figure 19(a). The indicated overshoot of 20 percent agrees with the predicted value.

A
4
1
8

The large-signal response can be roughly predicted by the switching time method. Values for t_{sw} versus $\Delta\varphi_e$ and $t_{\Delta\varphi_e}$ versus $\Delta\varphi_e$ obtained from equations (65) and (66) are plotted in figure 20. The curve of t_{sw} versus φ_{eo} comes from equation (76), where the value of C is found to be 0.992. It should be observed in figure 20 that for $\varphi_{eo} < 78$ seconds of arc, $\Delta\varphi_e$ is less than φ_{eo}. Hence, for a completely nonlinear system, no overshoot would be obtained and the response would be sluggish. It can be observed that the minimum possible settling time for $\varphi_{eo} = 60$ seconds of arc is about 3 seconds. The analog computer results presented in figure 19(b) show that the actual settling time is slightly over 5 seconds.

Experimental Results

The actual experimental results obtained for the platform response are presented in figure 21, which compares quite well with the analog computer results of figure 19. As shown in figure 21, transient response during the settling period was fast with very little overshoot, and tight control was maintained after the settling period. A long time history showed that the random error remained less than ±0.5 second of arc. This random error was probably caused by the random torque inputs. The small ripple in figure 20(a) is due to electrical noise. The larger overshoot and longer settling time in figure 21(b) compared to figure 19(b) is probably due to initial wheel velocity. The other minor dissimilarities between figures 19 and 21 were not accounted for; however, some general comments about practical problems which cause differences between theory and experiment may be made.

Any unbalance or pendulosity remaining in the platform after balancing produces a steady torque which may aid, but usually hinders, tracking. Misalinement of the sensor relative to the center of platform rotation causes cross coupling, so that the roll motion allowed about the line-of-sight axis couples through the other two axes and changes the pointing direction of the line-of-sight axis. Electrical delays add small lag

terms to the open-loop equations, but they are generally negligible for the systems considered here. The effects of saturation in the sensor and in the motor amplifier have already been discussed. Although hysteresis and dead zone have no obvious effects in the experimental results for the error-network system, they deserve some consideration. Some computer results were obtained by modifying the circuit of figure 7 to include hysteresis and dead zone in the sensor, gyro, and motor amplifier. It was found that hysteresis in any of these components caused limit-cycle response. Furthermore, limit cycles resulted from dead zone in the gyro. A dead zone in the sensor helped to stabilize the system, but it resulted in a steady-state error as large as the dead zone. A dead zone in the motor amplifier had very little effect on the transient response, but it also produced a steady-state error as large as the dead zone.

The results for the rate-gyro system should also be mentioned. The large-signal response was essentially the same as for the error-network system, as predicted in the analytical discussion. However, the small-signal response was dominated by limit-cycle operation, which resulted from the rate-gyro dead zone. The threshold of the gyros was about 30 seconds of arc/second, and the error amplitude of the resulting limit cycle was ±5 seconds of arc.

CONCLUSIONS

To design some reasonable systems for precise attitude control of a satellite, several methods of damping were first considered to provide the necessary compensation. It has been shown theoretically that either a rate gyro or an error-rate network is suitable without modification, but that a tachometer must be connected in series with a high-pass filter in order to keep the error signal from building up with wheel speed.

The effects of adding an integrator to the control loop in order to minimize the error have been considered, and it has been shown that, for the requirements of the Orbiting Astronomical Observatory and other similar applications, the use of an integrating gyro (or electronic integrator) requires a much larger motor than would otherwise be necessary.

Of the various possible control systems considered, three were selected for a detailed analysis. The three systems, which differ only by the method of damping, are referred to as the rate-gyro, error-network, and tachometer systems; the tachometer system includes a high-pass filter.

An analytical investigation, which consisted of a generalized linear analysis, a nonlinear analysis using the switching-time method, and an analog computer study, showed that all three systems were theoretically capable of producing adequate response and also of maintaining the required pointing accuracy for the Orbiting Astronomical Observatory of ±0.1 second of arc. Practical considerations and an experimental investigation using laboratory apparatus showed, however, that the error-network system was

superior to the other two. The rate-gyro system was shown to be inferior because the threshold level causes a significant amount of limit-cycle operation. The tachometer system was shown to be inferior because a device with the required dynamic range of operation does not appear to be available; the response is sluggish for low limits on the sensor output; and the large amount of tachometer feedback had a significant effect on the pointing error due to disturbance torque. For the error-network system, experimental data taken under laboratory conditions with relatively large extraneous disturbances show that a dynamic tracking error of less than ±0.5 second of arc was obtained.

Ames Research Center
National Aeronautics and Space Administration
Moffett Field, Calif., Nov. 16, 1960

APPENDIX A

VELOCITY AND TORQUE INPUTS

In this appendix the velocity and torque inputs that will be encountered during stellar observations by the Orbiting Astronomical Observatory are briefly described.

VELOCITY INPUTS

The line-of-sight velocity inputs consist of parallax and aberration components which result from the motion of the satellite relative to the earth and from the motion of the earth relative to the sun.

Velocity aberration occurs because the velocity of the satellite is a significant fraction of the velocity of light, as illustrated in the sketch. The aberration angle is a maximum when the satellite velocity is

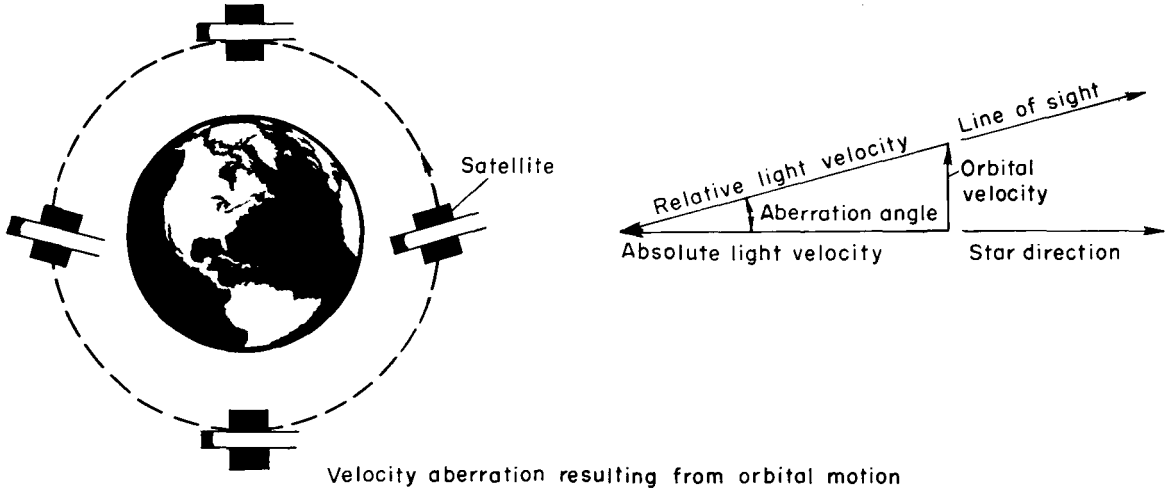

Velocity aberration resulting from orbital motion of a satellite about the Earth

Sketch (k)

perpendicular to the light velocity. For a 500-mile circular orbit having a period of 100 minutes, the satellite velocity is 4.72 miles/second. The maximum aberration angle found by taking the ratio of satellite velocity to the velocity of light is 2.54×10^{-5} radian or about 5 seconds of arc. Since the aberration angle is sinusoidal at orbital frequency, the maximum line-of-sight velocity is found by multiplying the maximum aberration angle by the angular frequency, which gives 1.6×10^{-6} radian/minute = 0.005 second of arc/second. This component of line-of-sight velocity due to aberration is very much larger than the component resulting from the motion of the earth about the sun, which may be completely neglected.

Parallax, which is the difference in direction of a body when viewed from different places, may also be completely neglected, because of the large distances which separate the earth from the stars.

TORQUE INPUTS

The disturbance torques acting on an earth satellite result largely from the earth's gravity gradient, the sun's radiation pressure, the earth's atmospheric density, and the earth's magnetic field. Only the order of magnitude of these torques will be discussed here; a more detailed discussion may be found in reference 1. The torque due to the earth's gravity gradient has been frequently discussed. For the astronomical satellite, a one percent inertia unbalance could result in a torque whose amplitude varies at twice orbital frequency between zero and 160 dyne cm with an average value of 80 dyne cm about one axis.

A 4 1 8 Solar radiation causes a significant torque if the body is geometrically unsymmetrical or if the surface materials have different reflectivities so that the pressure center is not in line with the mass center when viewed from different angles. Using a solar pressure of 7×10^{-5} dyne/cm^2 for a body of medium reflectivity, a torque of 100 dyne cm will be produced on an exposed surface area of 100 square feet if the pressure and mass centers differ by about 15 cm or 1/2 foot.

Atmospheric density torque may be treated in the same manner as solar radiation, since both effects are calculated using the distance between the center of pressure and the center of mass. For the 500-mile orbit being considered, the dynamic pressure is roughly 1.5×10^{-5} dyne/cm^2, resulting in a torque which is somewhat smaller than the solar torque. However, if the altitude were reduced to 400 miles, the atmospheric torque would increase by a factor of about seven, so that it might well be the largest disturbance torque.

When the earth's magnetic field interacts with the net magnetic field of the satellite, another unwanted torque is produced. Since the field of the satellite is produced by all of the magnetic materials and circulating loop currents distributed throughout the satellite, the resulting torque is very difficult to estimate. Although large torques could result from this source, they may be significantly reduced by nonmagnetic design and symmetrical distribution of components.

APPENDIX B

ANALYSIS OF AN INTEGRATING-GYRO SYSTEM

In this appendix an integrating-gyro system will be compared to the rate-gyro, error-network, and tachometer systems. It will be shown that although a lower outer loop gain is allowable, a much larger motor is required by stability and error requirements for the Orbiting Astronomical Observatory and other similar applications. For this analysis the closed-loop response equation and the closed-loop error equation will be examined. These equations for the integrating gyro may be obtained directly from those for a rate gyro by replacing K_a by K_a/s. With this modification, equation (38) for closed-loop response becomes

$$\varphi_b = \frac{\left(\varphi_c + \frac{\omega_{1s}}{s}\right)\frac{K_e'}{\tau_m} - \frac{T_d}{J_b}\left(s + \frac{1}{\tau_m}\right)}{s^3 + \frac{1}{\tau_m}s^2 + \frac{K_g'}{\tau_m}s + \frac{K_e'}{\tau_m}} \tag{B1}$$

Applying Routh's criterion shows that the system is stable if

$$\tau_m < \frac{K_g'}{K_e'} \tag{B2}$$

In order to develop error criteria, the closed-loop error equation for an integrating gyro is obtained by replacing K_a by K_a/s in equation (4), giving

$$\varphi_e = \frac{(s\varphi_c + \omega_{1s})\left(s^2 + \frac{1}{\tau_m}s + \frac{K_g'}{\tau_m}\right) + \frac{T_d}{J_b}\left(s + \frac{1}{\tau_m}\right)}{s^3 + \frac{1}{\tau_m}s^2 + \frac{K_g'}{\tau_m}s + \frac{K_e'}{\tau_m}} \tag{B3}$$

The steady-state errors for step inputs are found by applying the final value theorem.

For $\varphi_c(s) = \varphi_c/s$ (with $\omega_{1s} = T_d = 0$),

$$\frac{\varphi_{ess}}{\varphi_c} = \lim_{s\to 0} s\varphi_e = 0 \tag{B4}$$

For $\omega_{1s}(s) = \omega_{1s}/s$ (with $\varphi_c = T_d = 0$),

$$\frac{\varphi_{ess}}{\omega_{1s}} = \frac{K_g'}{K_e'} \tag{B5}$$

For $T_d(s) = T_d/s$ (with $\varphi_c = \omega_{1s} = 0$),

$$\frac{\varphi_{ess}}{T_d} = \frac{1}{J_b}\frac{1}{K_e'} \tag{B6}$$

To establish one error criterion, equation (B5) can be written as

A
4
1
8

$$\frac{K_g'}{K_e'} \leq \frac{\varphi_{ess_{max}}}{\omega_{1s}} \tag{B7}$$

Incidently, this is identical to equation (28) for the rate gyro. For the Orbiting Astronomical Observatory the maximum ratio resulting from $\varphi_{ess_{max}} = 0.1$ second of arc and $\omega_{1s} = 0.01$ second of arc/second is $K_g'/K_e' = 10$ radians/(radian/second).

To establish another error criterion, equation (B6) may be written as

$$K_e' \geq \frac{T_d}{J_b}\frac{1}{\varphi_{ess_{max}}} \tag{B8}$$

The minimum allowable outer loop gain resulting from $\varphi_{ess_{max}} = 0.1$ second of arc $\cong 5\times10^{-7}$ radian, $T_d = 100$ dyne cm, and $J_b = 10^{10}$ gram cm^2 is $K_e' = 0.02$ (radian/second)/radian, which is much smaller than the outer loop gain required for the rate-gyro, error-rate network, or tachometer systems.

The stability requirement of equation (B2) may be combined with the error requirement of equation (B7) to determine the maximum allowable motor time constant. If K_g'/K_e' is chosen as its maximum of 10 radians/(radian/second) to allow τ_m to be as large as possible, then by equation (B2), τ_m must be less than 10 seconds. When the angular momentum due to disturbance torque has been determined from equation (30), the motor stall torque may be calculated by using equation (36). If J_w is selected as before as 10^3 gram cm^2 for $\omega_{w_{max}} = 6000$ rpm and τ_m is less than 10 seconds, then the stall torque may be written as the inequality, $T_{ms} > 6.3\times10^4$ dyne cm, or $T_{ms} > 0.9$ oz in. It should be emphasized that the minimum value of stall torque indicated here corresponds to a neutrally stable system having sustained oscillations. Actually, analog results and a detailed analysis indicate that to have reasonable damping

ratios, the stall torque must range from 3 to 10 oz in. and is therefore 10 to 30 times larger than the value of 0.3 oz in. determined for the rate-gyro, error-network, and tachometer systems. If weight and power must be conserved, the integrating-gyro system is not as promising as the others and therefore was not considered in detail in this report.

It should be observed that for the numerical example just considered, the motor size for the rate-gyro, error-network, and tachometer systems was determined from the settling-time requirement while the motor size for the integrating-gyro system was determined from the steady-state error and stability requirements. It must be conceded that the integrating-gyro system might compare favorably with the other three systems if a much shorter settling time were required, which is not likely for precise satellite attitude control, or if a much larger ratio of $\varphi_{ess_{max}}$ to ω_{1s} in equation (B7) were allowed, which is entirely possible for some applications.

APPENDIX C

COMPLETE MOTOR AND WHEEL BLOCK DIAGRAM

A complete block diagram of the motor-wheel combination for controlling satellite attitude is shown in the sketch. Here B_e is the

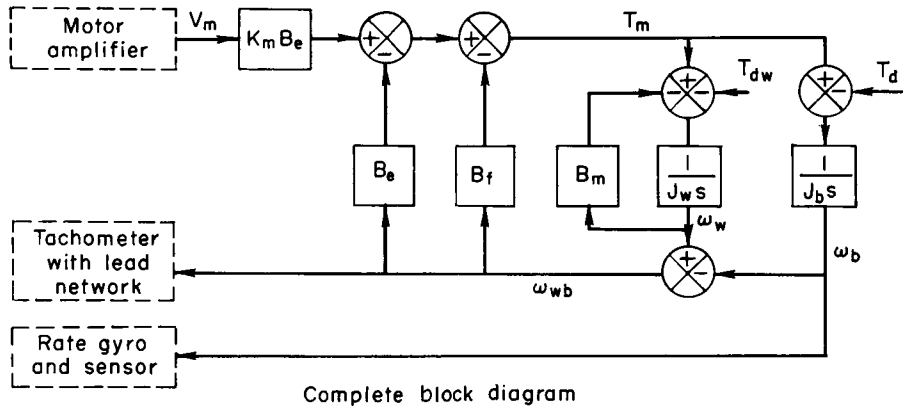

Complete block diagram of motor-wheel combination

Sketch (1)

back emf constant, $K_m B_e$ is the forward voltage constant, B_f is a viscous friction constant, and B_m is a magnetic torque constant resulting from the earth's magnetic field. The externally applied wheel torque, T_{dw}, is composed of such effects as gravity torques on an unbalanced wheel, and it is completely negligible.

The wheel velocity, ω_w, resulting from $T_m - T_{dw}$ is relative to inertial space, as also is the body velocity, ω_b, resulting from $T_m - T_d$. The wheel velocity relative to the body, ω_{wb}, is actually equal to ω_w minus ω_b. However, since the body inertia is so much larger than the wheel inertia, ω_{wb} can be approximated by ω_w.

Neglecting T_{dw} and approximating ω_{wb} by ω_w, the motor-wheel transfer function becomes,

$$\frac{T_m}{V_m} = \frac{\dfrac{K_m B_e (B_m + J_w s)}{B_e + B_f + B_m}}{1 + \dfrac{J_w s}{B_e + B_f + B_m}} \qquad (C1)$$

After the magnetic torque constant, B_m, which is very small, and the viscous friction constant, which is relatively insignificant, are neglected the transfer function reduces to the following form:

$$\frac{T_m}{V_m} = \frac{K_m J_w s}{1 + \frac{J_w}{B_e} s} \tag{C2}$$

This form is used in sketches (b), (c), and (d) with J_w/B_e replaced by the motor time constant, τ_m.

A useful equation for the motor time constant may be derived by using the following approximate equation taken from the sketch:

$$T_m = K_m B_e V_m - B_e \omega_w \tag{C3}$$

A 4 1 8

By setting $\omega_w = 0$ and $V_m = V_{m_{max}}$, the stall torque is obtained.

$$T_{ms} = K_m B_e V_{m_{max}} \tag{C4}$$

and by setting $T_m = 0$, $V_m = V_{m_{max}}$, and $\omega_w = \omega_{w_{max}}$, equation (C3) gives

$$B_e \omega_{w_{max}} = K_m B_e V_{m_{max}} \tag{C5}$$

By combining equations (C4) and (C5) it is found that

$$B_e = \frac{T_{ms}}{\omega_{w_{max}}} \tag{C6}$$

When this relation is used, the equation for τ_m becomes

$$\tau_m = \frac{J_w \omega_{w_{max}}}{T_{ms}} \tag{C7}$$

This form is used in equation (36) of the report.

REFERENCES

1. Triplett, William C.: Design Considerations for an Orbiting Astronomical Observatory. ARS Paper 1184-60.

2. Schmidt, Stanley F.: The Analysis and Design of Continuous and Sampled-Data Feedback Control Systems With a Saturation Type Nonlinearity. NASA TN D-20, 1959.

3. Truxal, John G.: Control System Synthesis. McGraw-Hill Book Co., Inc., 1955.

TABLE I.- TABLE OF GENERALIZED LINEAR PARAMETERS AND SIMPLIFYING ASSUMPTIONS

SYSTEM	ω_n	ζ	$\frac{1}{\tau_1\omega_n}$	$\frac{1}{\tau_2\omega_n}$	Simplifying assumptions	Equation numbers
Rate-gyro	$\sqrt{\frac{K_e'}{\tau_m}}$	$\frac{K_g'}{2\sqrt{\tau_m K_e'}}$	∞	$\frac{1}{\sqrt{\tau_m K_e'}}$	$K_g' \gg 1$	28
Error-network	$\sqrt{\frac{K_e'}{\tau_m}}$	$\frac{K_i'}{2\sqrt{\tau_m K_e'}}$	$\frac{\sqrt{\tau_m K_e'}}{K_i'}$	$\frac{1}{\sqrt{\tau_m K_e'}}$	$K_i' \gg 1$ $\tau_m \gg \tau_d \ll \frac{K_i'}{K_e'}$ $\tau_d \ll \sqrt{\frac{\tau_m}{K_e'}}$	43 44, 45 50
Tachometer	$\sqrt{\frac{K_e'}{K_t'}}$	$\frac{\tau_t}{2}\sqrt{\frac{K_e'}{K_t'}}$	$\frac{1}{\tau_t}\sqrt{\frac{K_t'}{K_e'}}$	$\frac{1}{\sqrt{K_t' K_e'}}$	$K_e' \gg \frac{1}{\tau_t}$ $K_t' \gg \tau_m + \tau_t$ $\frac{\tau_t \tau_m}{K_t'} \ll \sqrt{\frac{K_t'}{K_e'}}$	52 53 58

TABLE II.- TABLE OF SUBSTITUTIONS FOR THE GENERALIZED LINEAR PARAMETERS AND SIMPLIFYING ASSUMPTIONS USING THE NUMERICAL EXAMPLE

SYSTEM	ω_n(radians/sec)	ζ	$\frac{1}{\tau_1 \omega_n}$	$\frac{1}{\tau_2 \omega_n}$	Simplifying assumptions	$\frac{K_g'}{K_e'}, \frac{K_i'}{K_e'}$ or $\frac{K_t'}{K_e'}$ $\left(\frac{\text{radians}}{\text{radian/sec}}\right)$	τ_d or τ_t (sec)
Rate-gyro	2.24	.7	∞	.015	94 >> 1	.625	
Error-network	2.24	.7	.7	.015	94 >> 1 30 >> .01 << .625 .01 << .446	.625	.01
Tachometer (Case A)	2.24	.7	.7	.015	150 >> 1.6 30 >> 30.6 .625 << .446	.2	.625
Tachometer (Case B)	.224	.56	.9	.0015	150 >> .2 3,000 >> 35 0.05 << 4.46	20	5

Page intentionally left blank

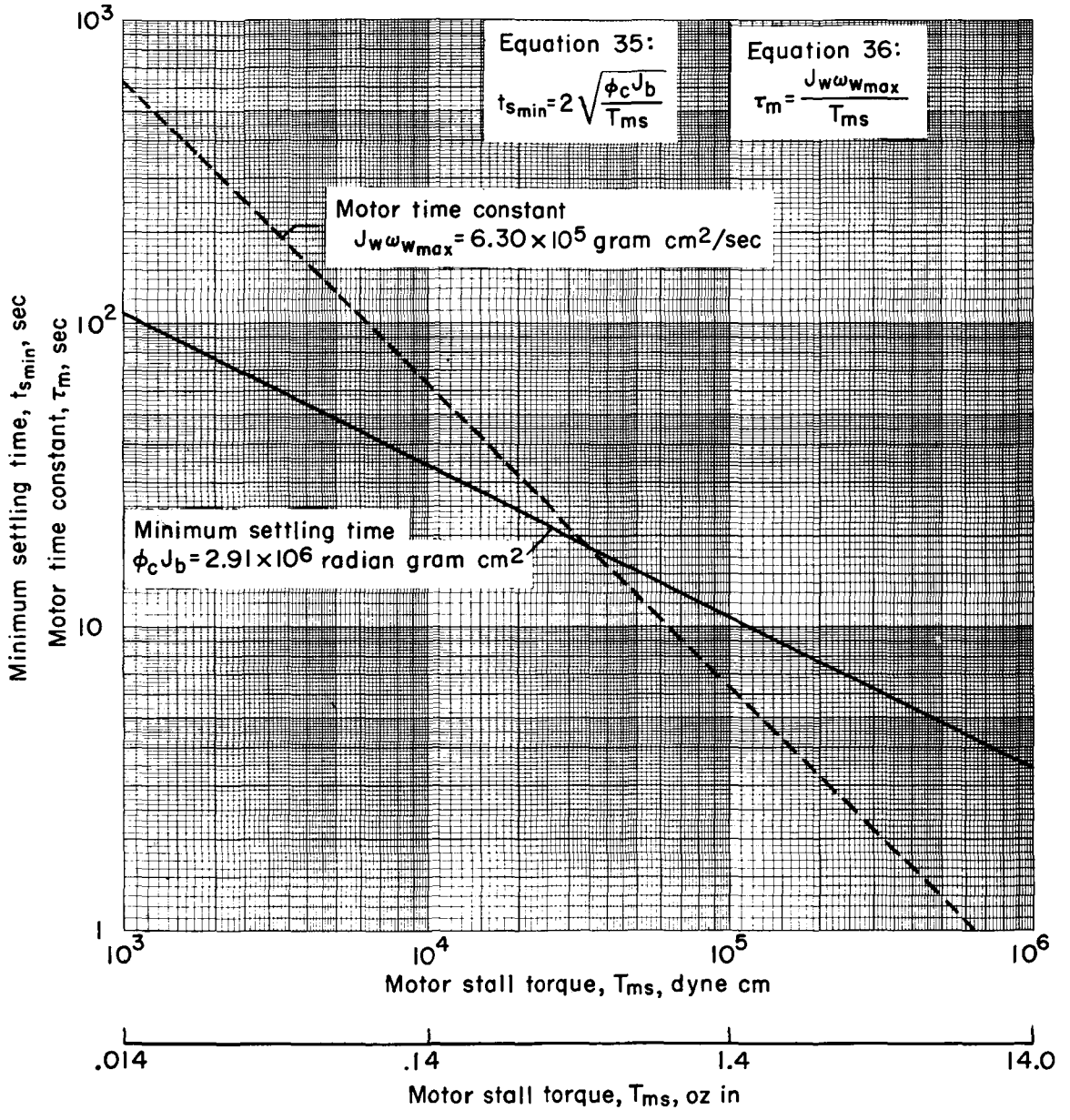

Figure 1.- Minimum settling time and motor time constant versus motor stall torque.

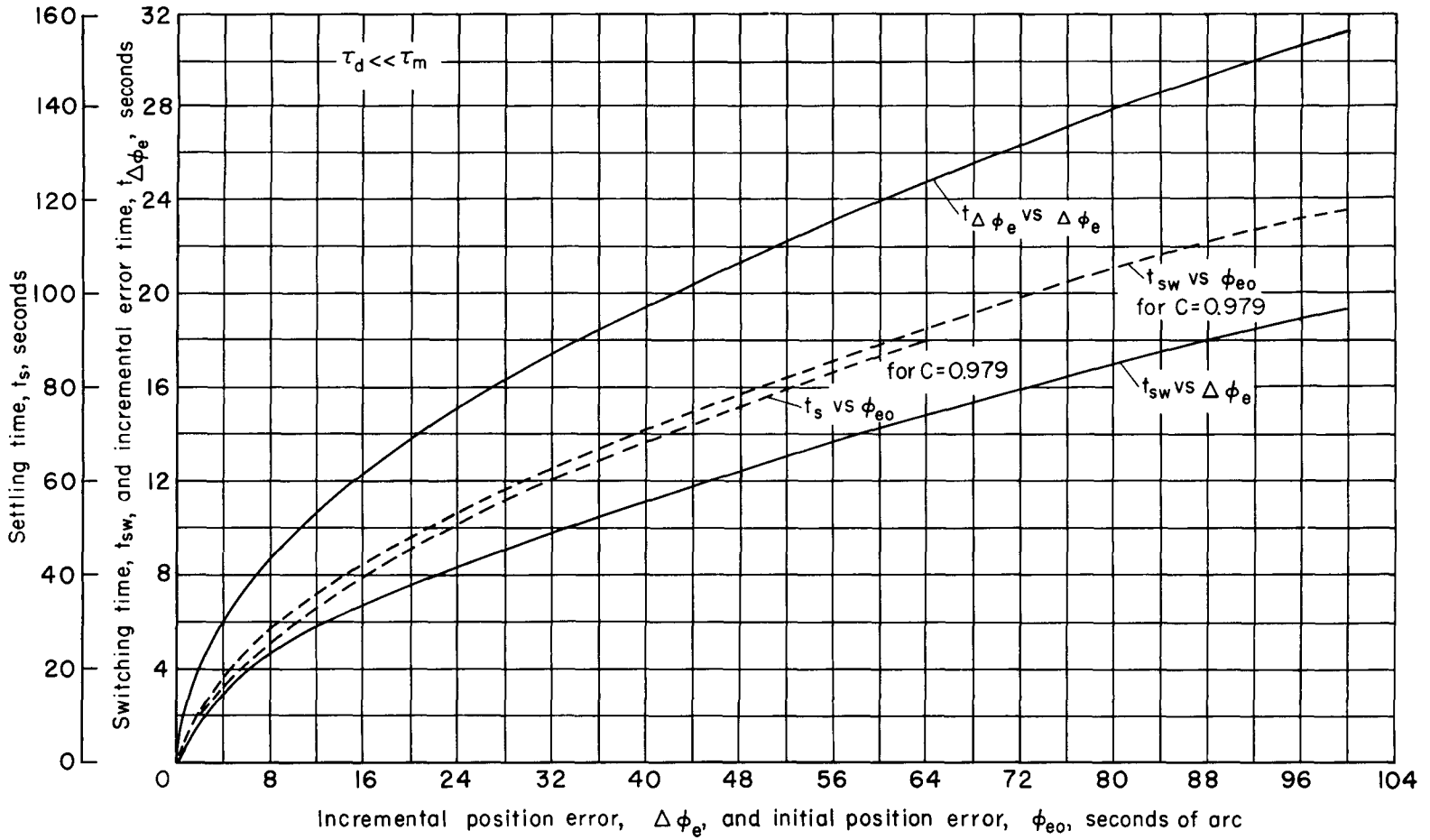

Figure 2.- Switching- and settling-time curves for rate-gyro and error-network systems.

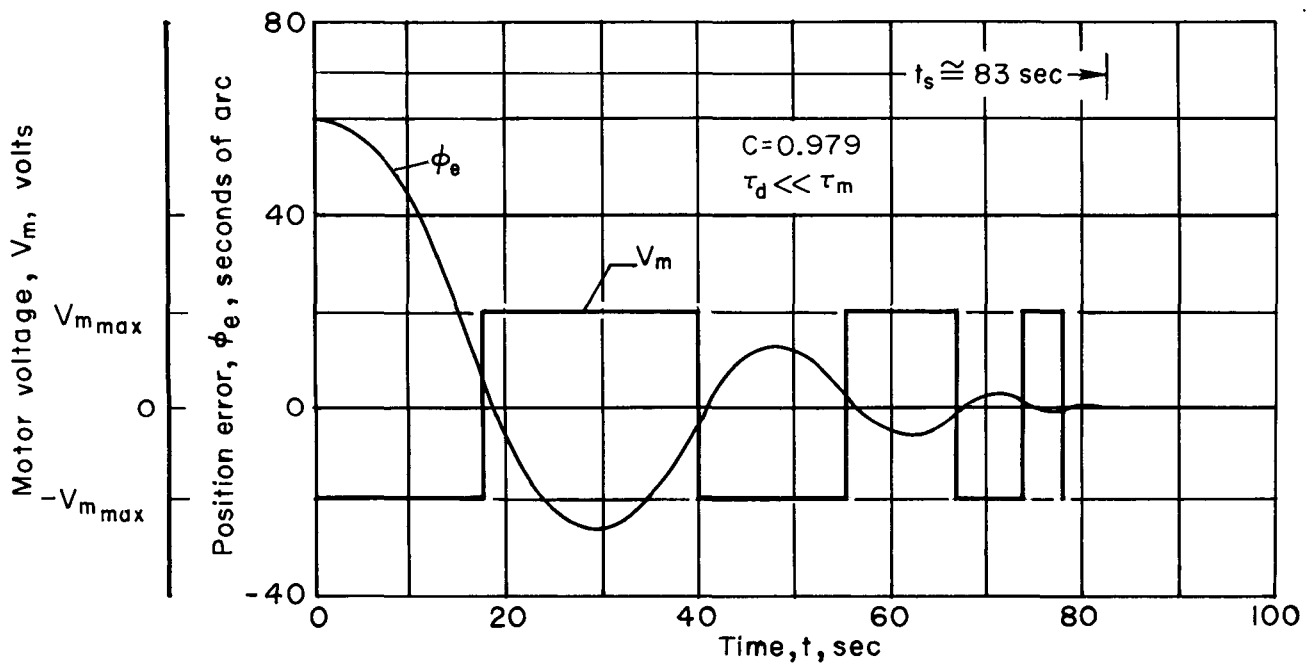

Figure 3.- Transient response and motor voltage curves for rate-gyro and error-network systems.

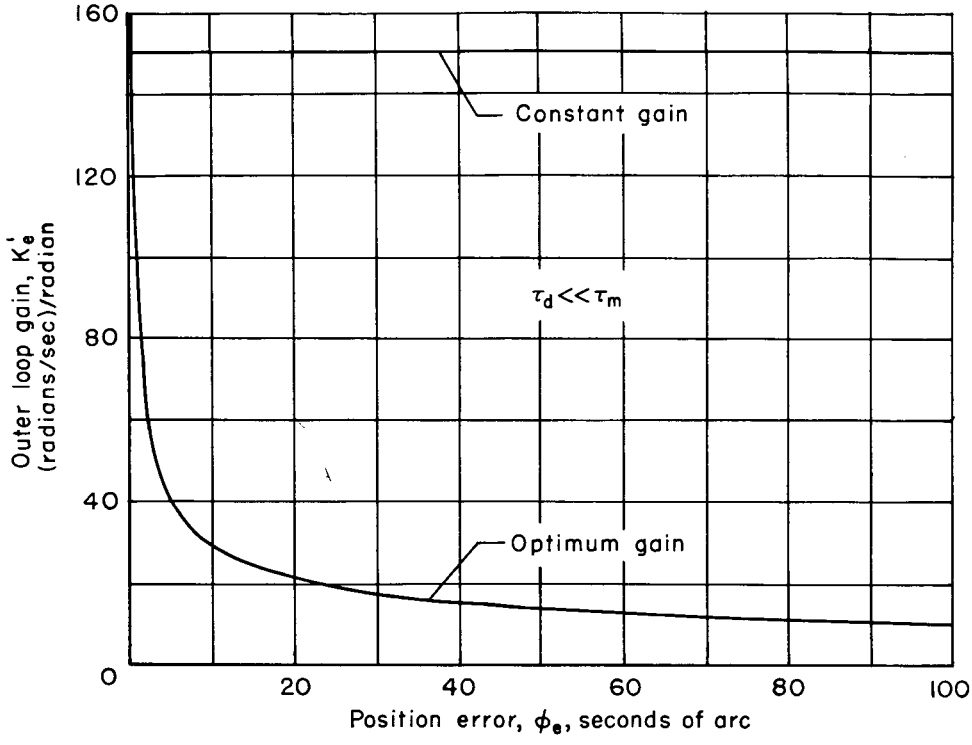

(a) Outer loop gain.

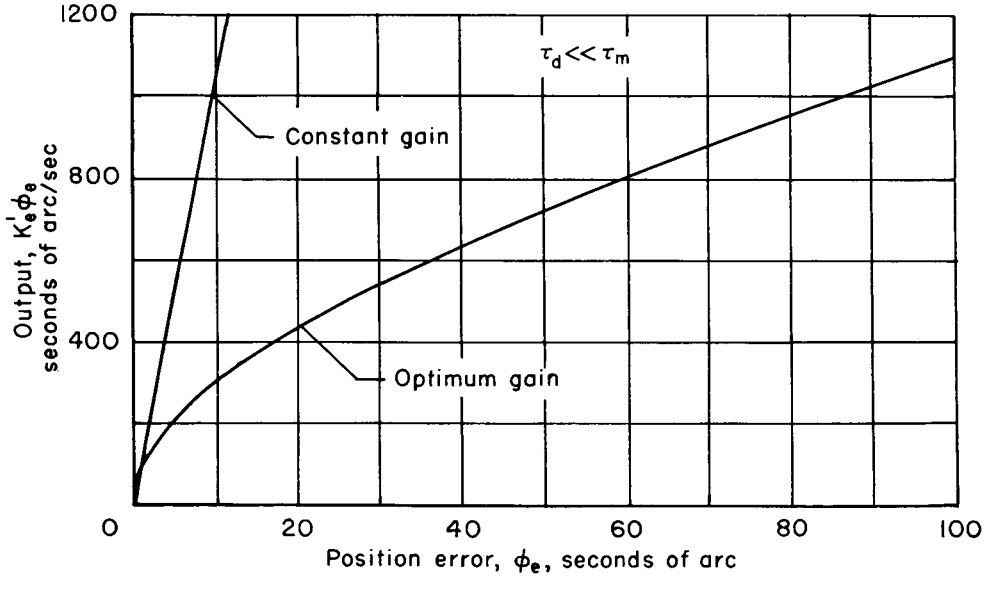

(b) Output.

Figure 4.- Outer loop gain and output of error amplifier for rate-gyro, and error-network systems.

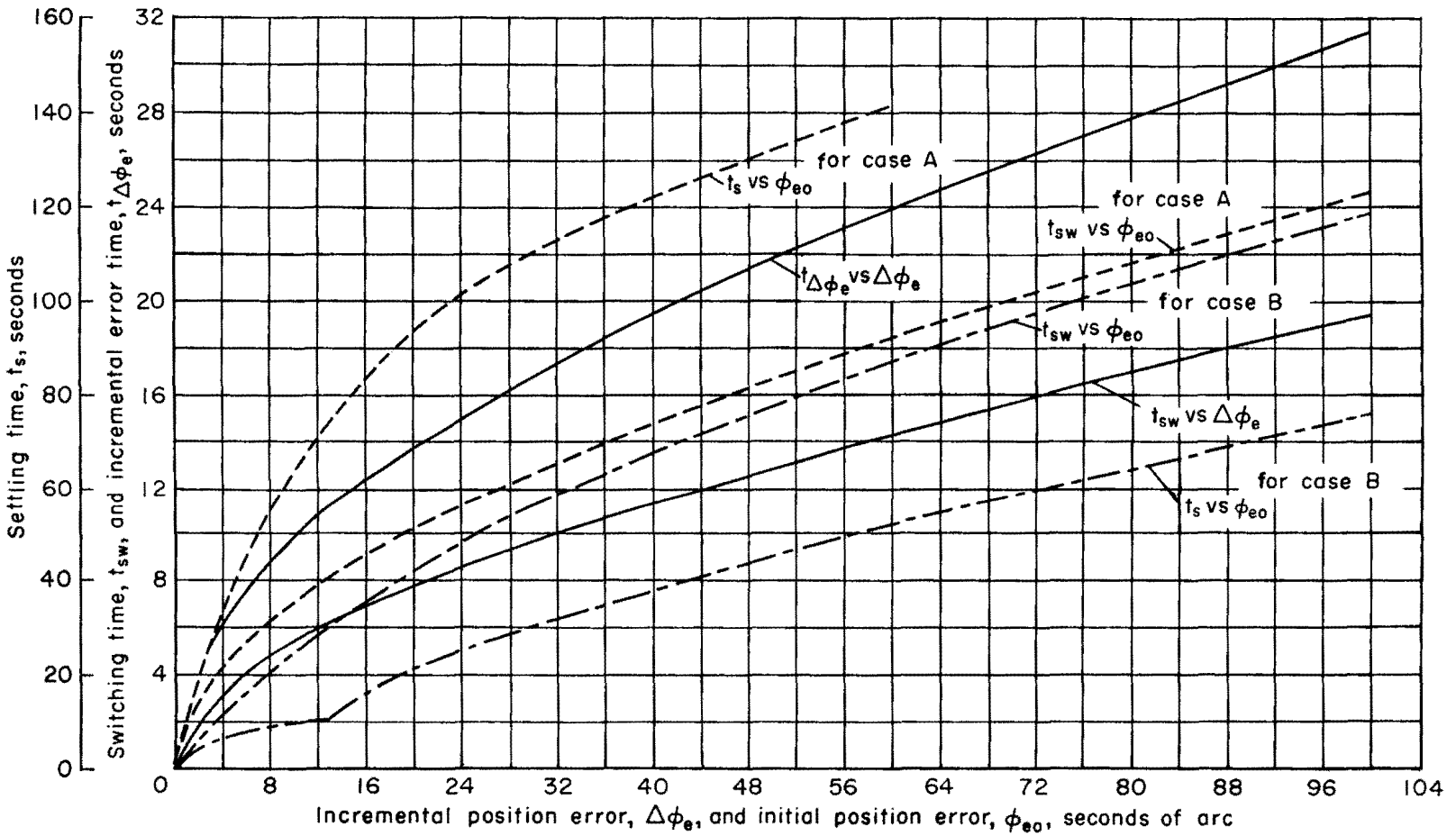

Figure 5.- Switching- and settling-time curves for tachometer system.

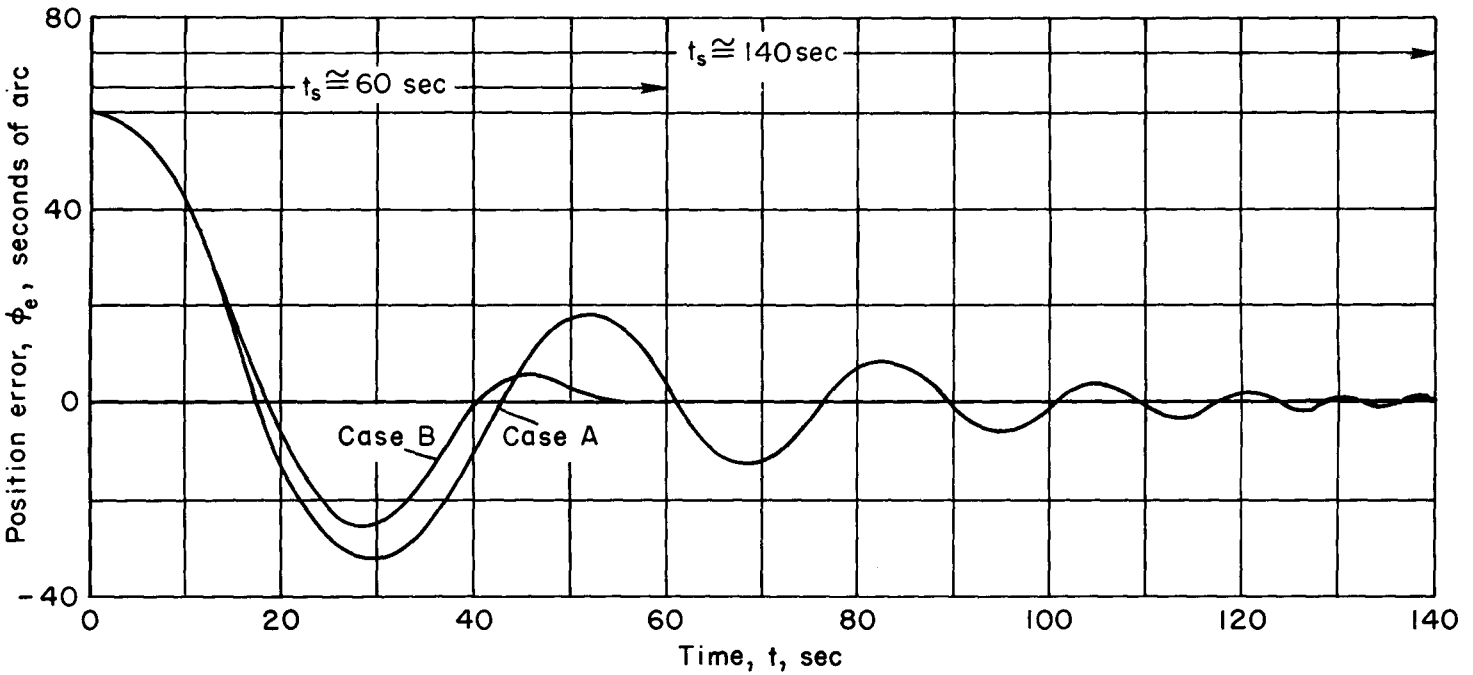

Figure 6.- Transient response curves for tachometer system.

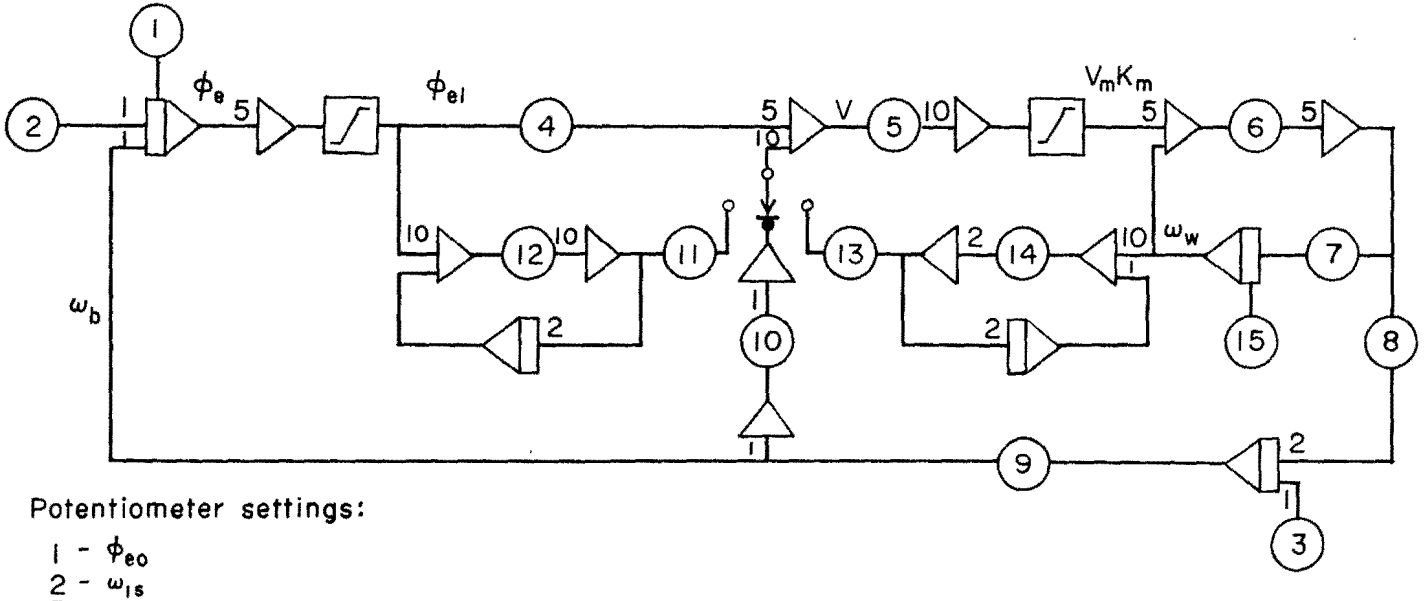

Potentiometer settings:

1 - ϕ_{eo}
2 - ω_{is}
3 - T_d/J_b
4 - $K_e/3.125$
5 - $K_a K_m/2\times10^{-11}$
6 - $10/\tau_m$
7 - 0.04
8 - $2\times10^6 J_w/J_b$
9 - 0.1
10 - $K_g/2.5$
11 - $K_i/6.25$
12 - $0.01/T_d$
13 - $4\times10^5 K_t$
14 - $0.5/\tau_t$
15 - ω_{wo}

Scales:

ϕ_{eo}	3×10^{-6} radians/volt
ϕ_e	3×10^{-6} radians/volt
ϕ_{el}	6×10^{-7} radians/volt
V	3.75×10^{-7} volts/volt
V_mK_m	75 radians/sec/volt
ω_b	1.5×10^{-6} radians/sec/volt
ω_{is}	1.5×10^{-6} radians/sec/volt
T_d/J_b	7.5×10^{-8} radians/sec^2/volt
ω_w	15 radians/sec/volt
ω_{wo}	15 radians/sec/volt

Note: Double time scale was used

Figure 7.- Analog computer circuit with selector switch for rate-gyro, error-network, and tachometer systems.

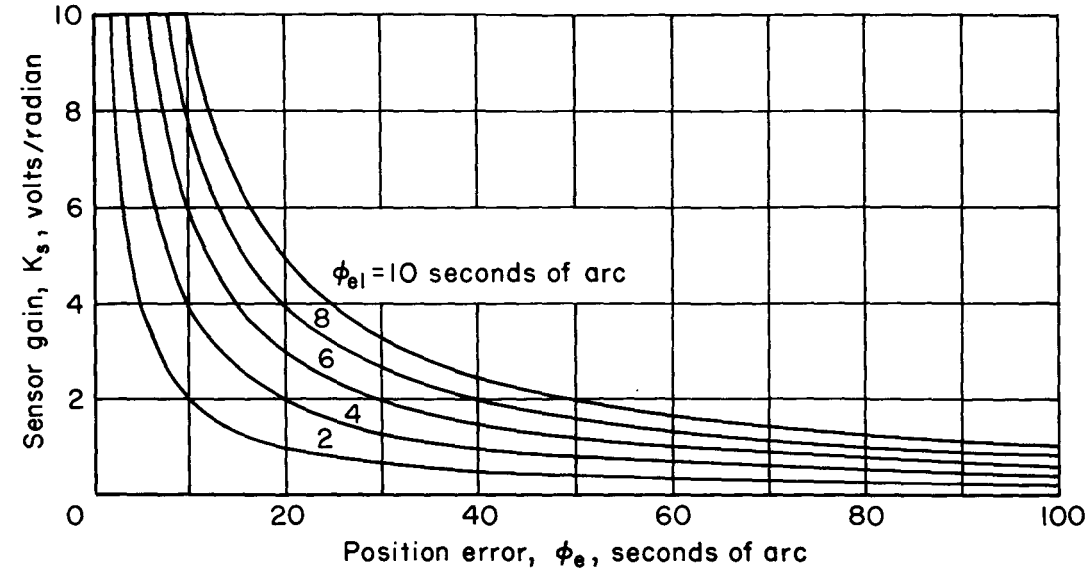

(a) Sensor gain.

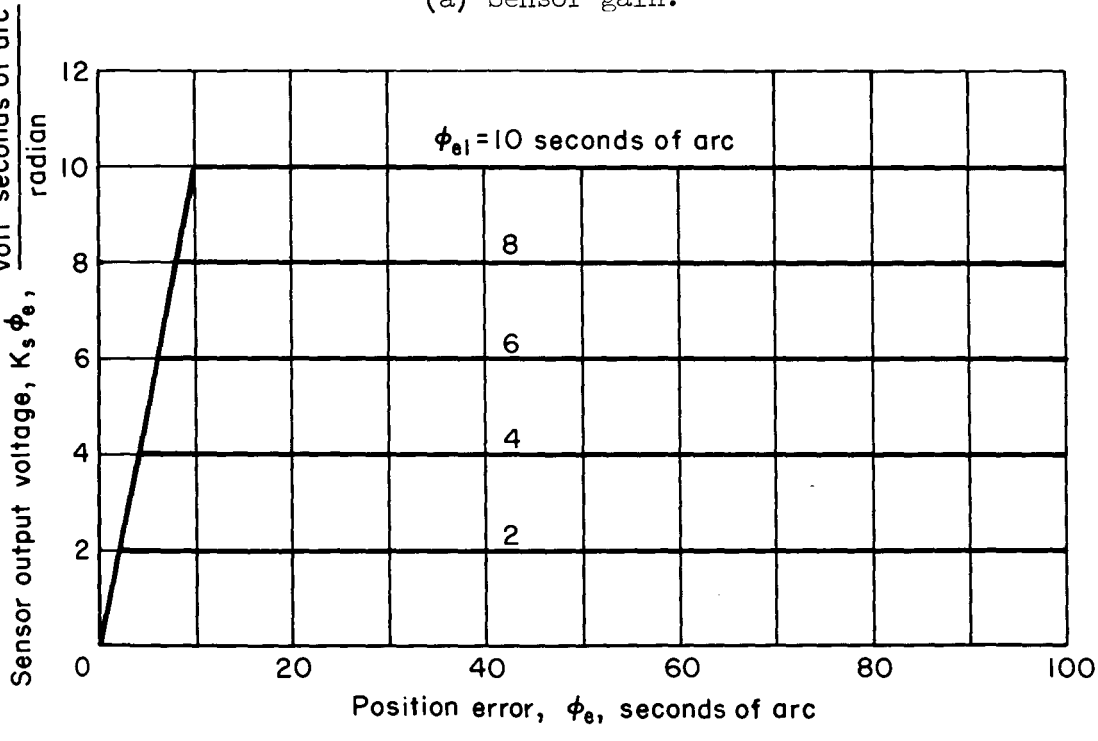

(b) Sensor output.

Figure 8.- Gain and output of sensor for analog computer simulation.

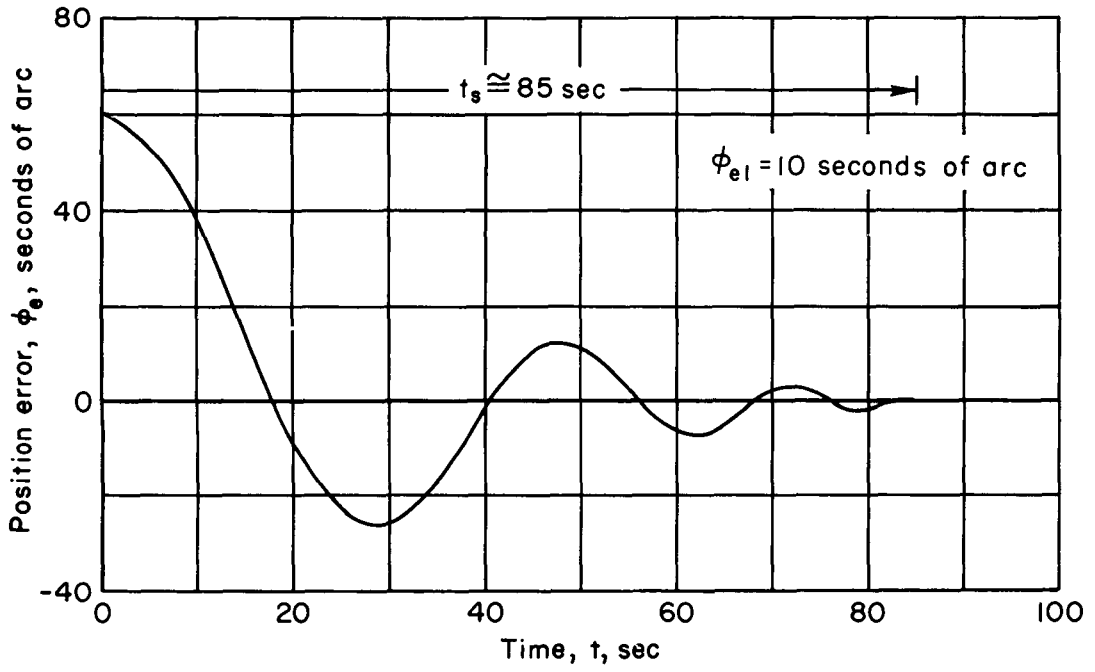

Figure 9.- Transient response curve for rate-gyro and error-network systems as simulated by analog computer.

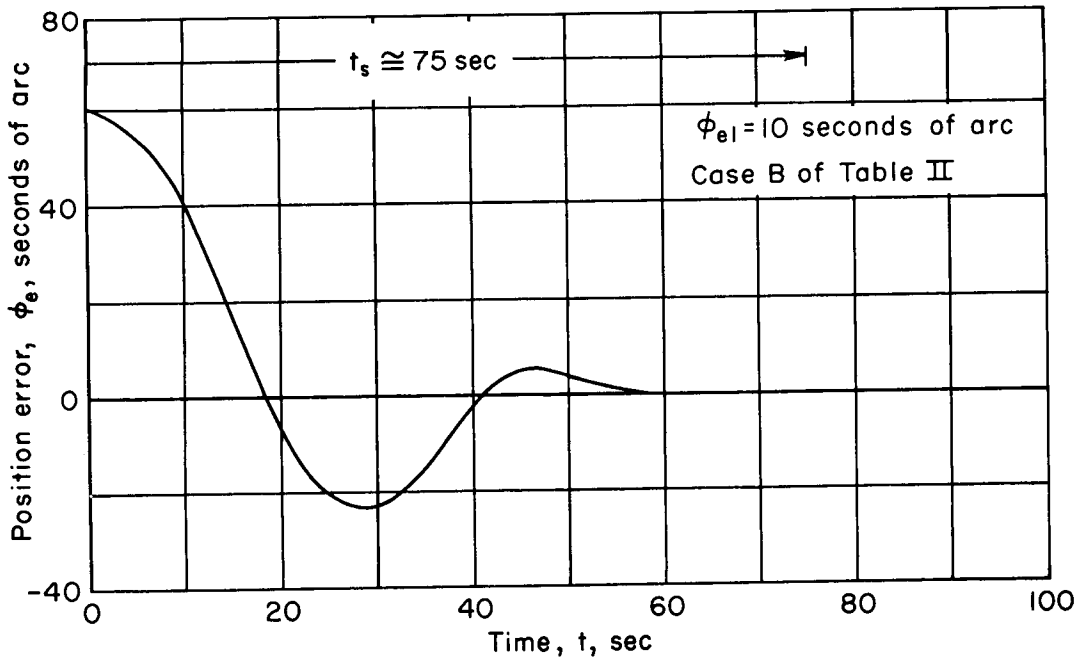

Figure 10.- Transient response curve for tachometer system as simulated by analog computer.

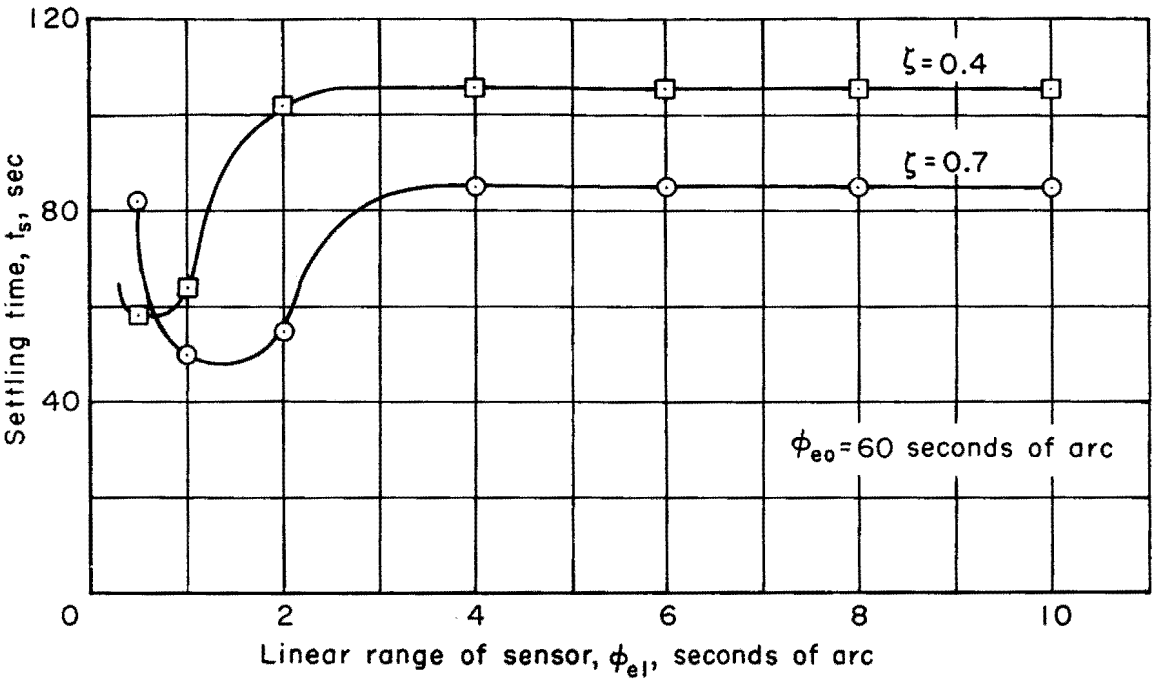

Figure 11.- Settling time versus linear range of sensor for rate-gyro system.

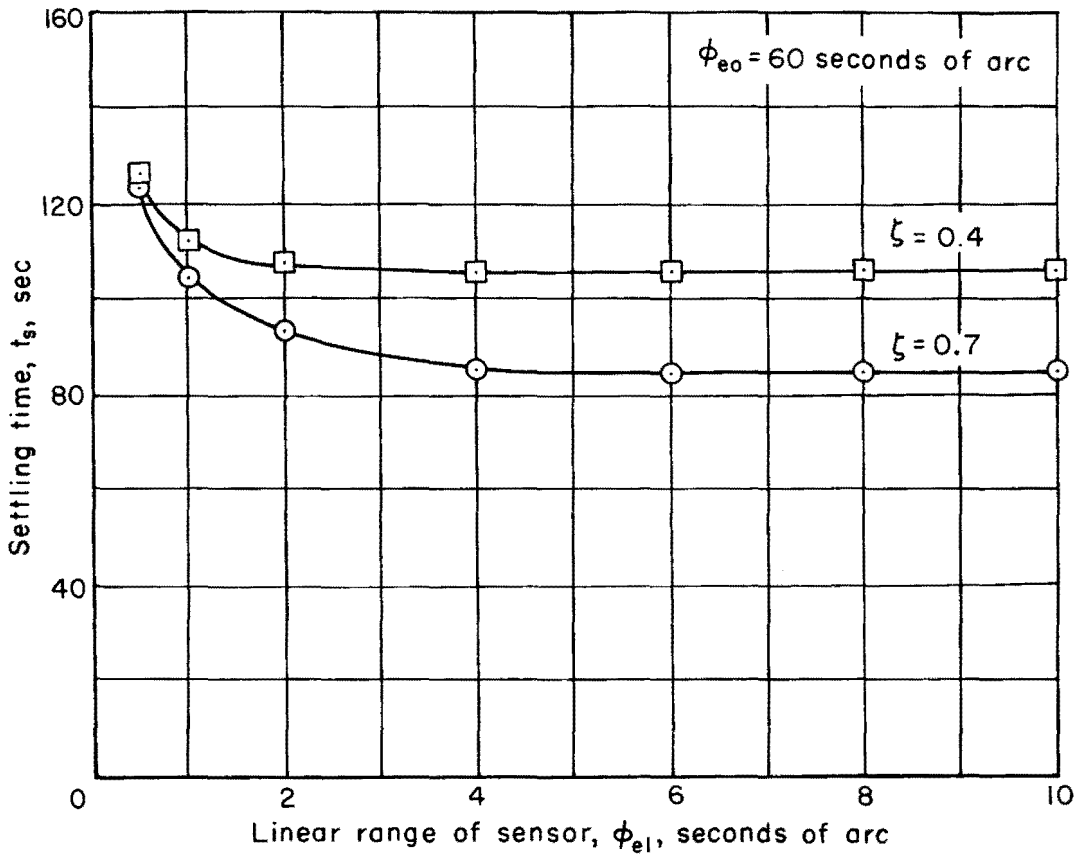

Figure 12.- Settling time versus linear range of sensor for error-network system.

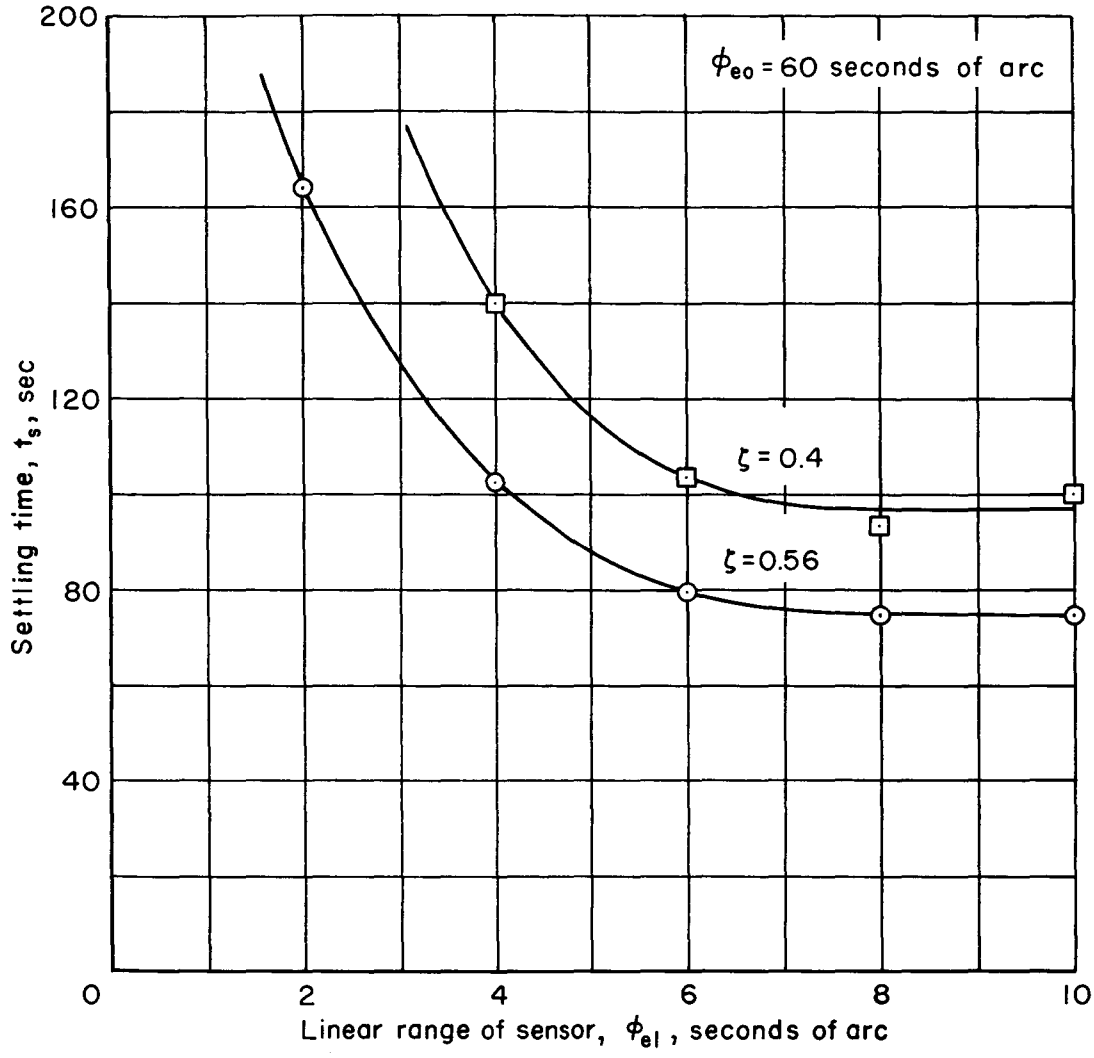

Figure 13.- Settling time versus linear range of sensor for tachometer system.

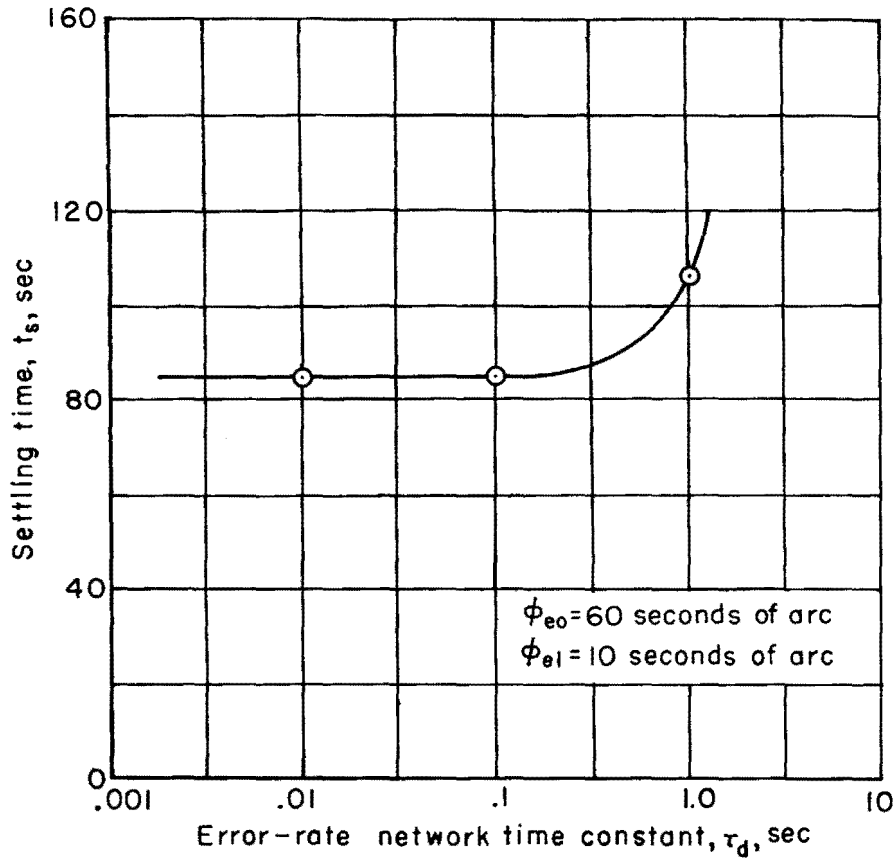

Figure 14.- Settling time versus error-rate network time constant for error-network system.

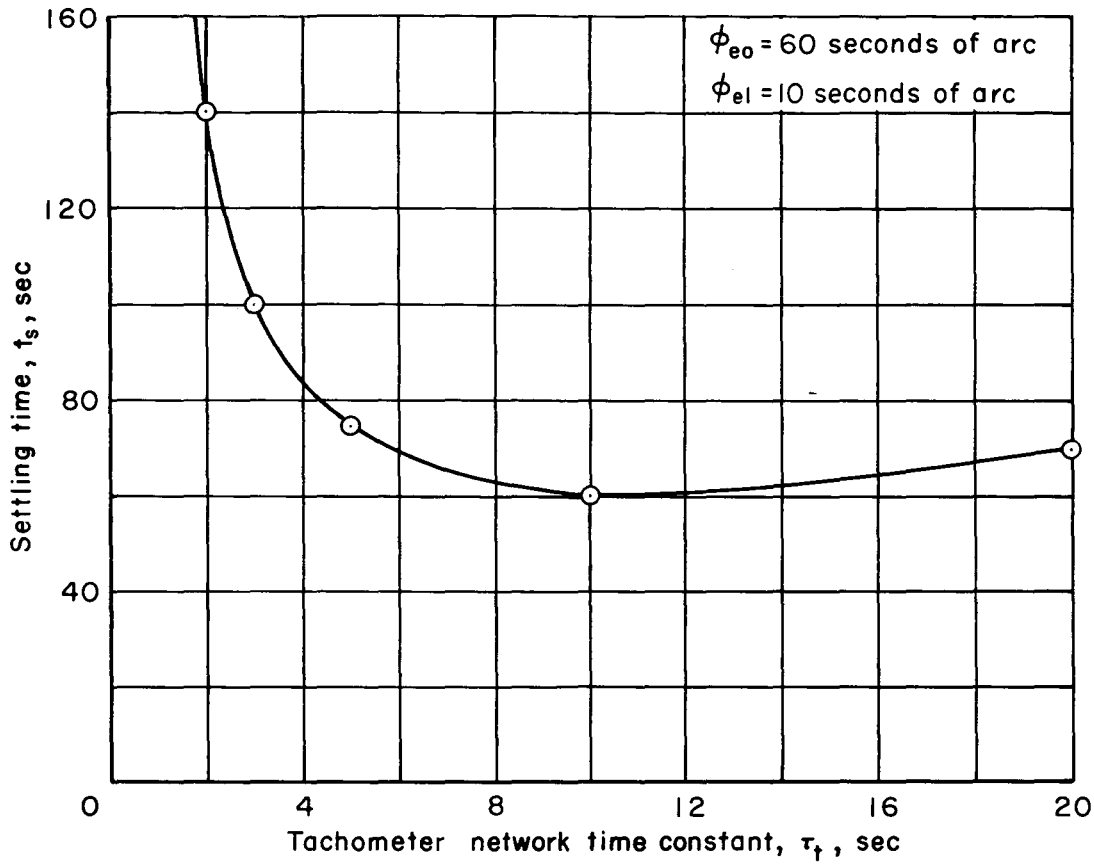

Figure 15.- Settling time versus tachometer network time constant for tachometer system.

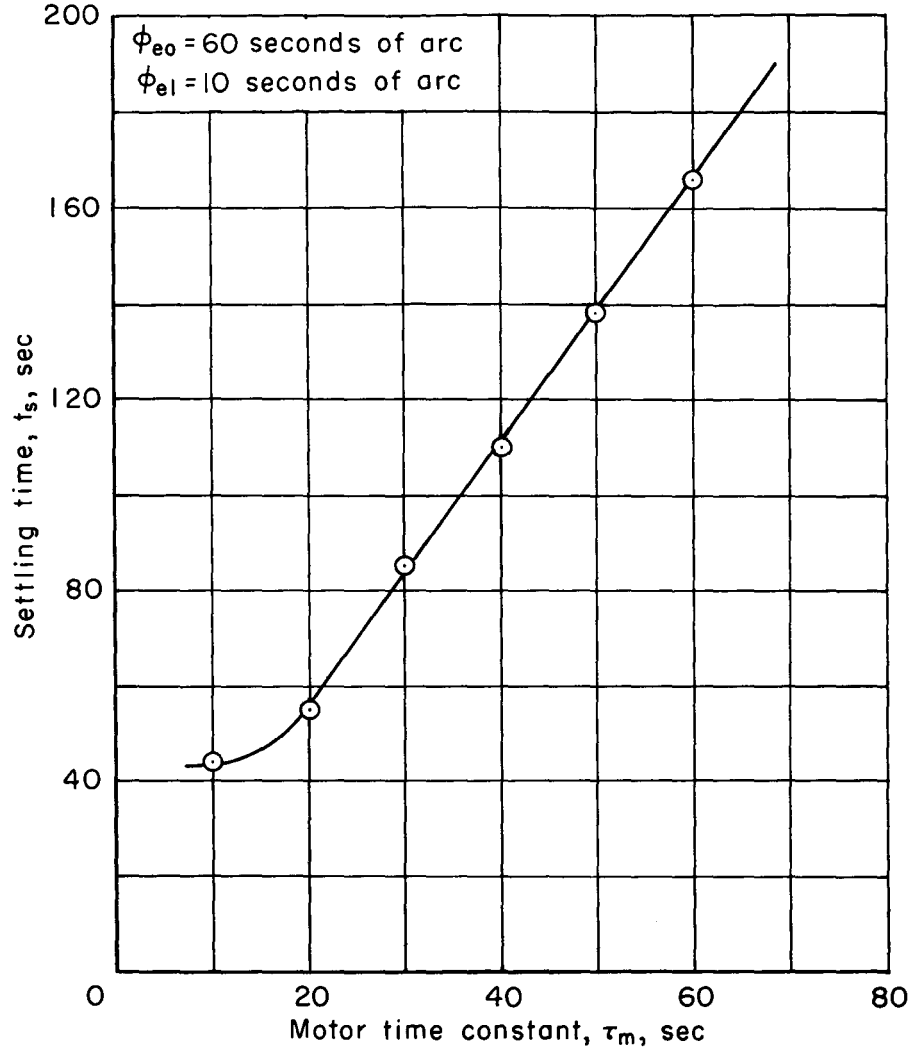

Figure 16.- Settling time versus motor time constant for rate-gyro and error-network systems.

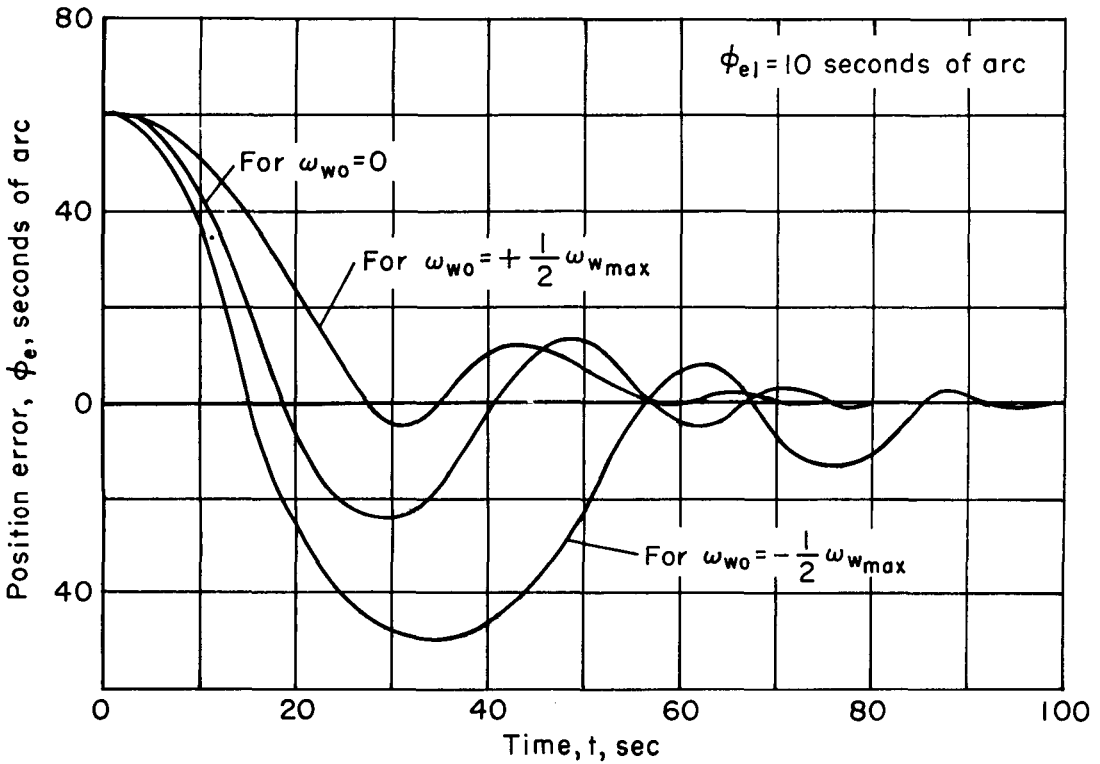

Figure 17.- Transient response curves showing effect of initial wheel speed for rate-gyro and error-network systems as simulated by analog computer.

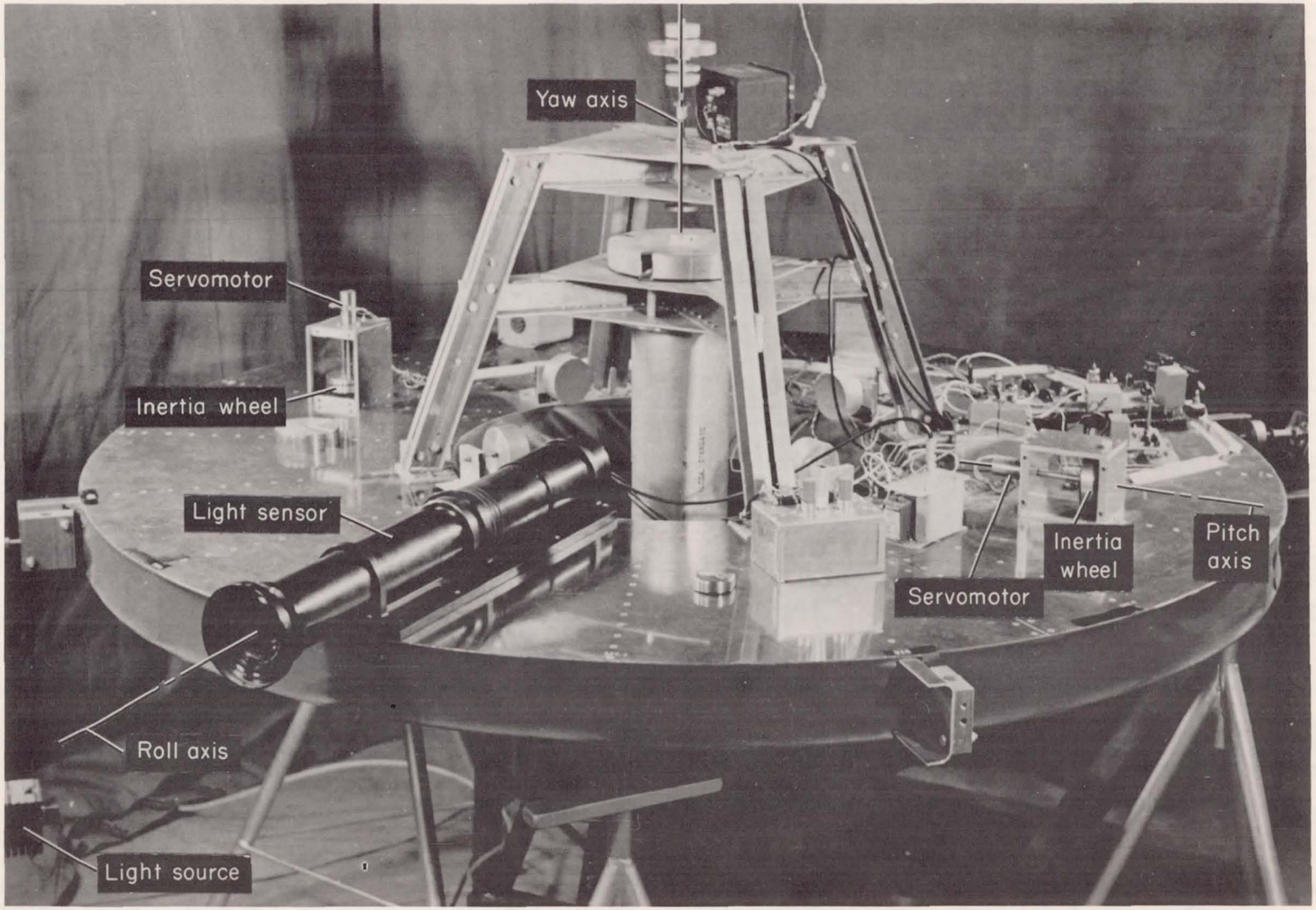

Figure 18.- Laboratory apparatus for experimental testing.

A-26244.2

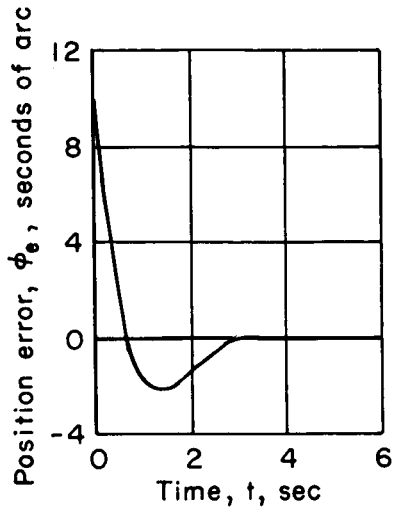

(a) Small-signal response.

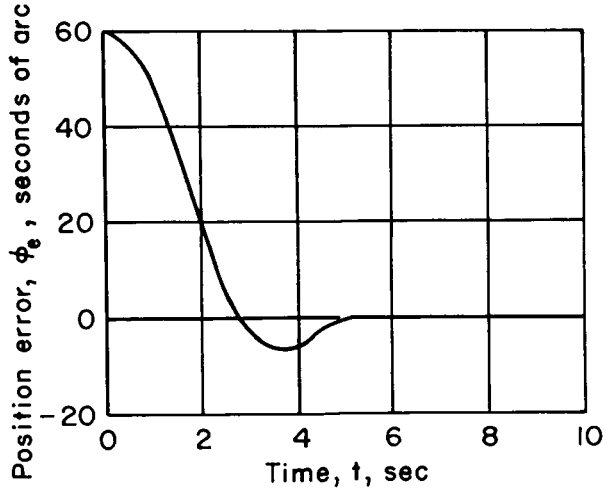

(b) Large-signal response.

Figure 19.- Small- and large-signal transient response curves for error-network system as simulated by analog computer.

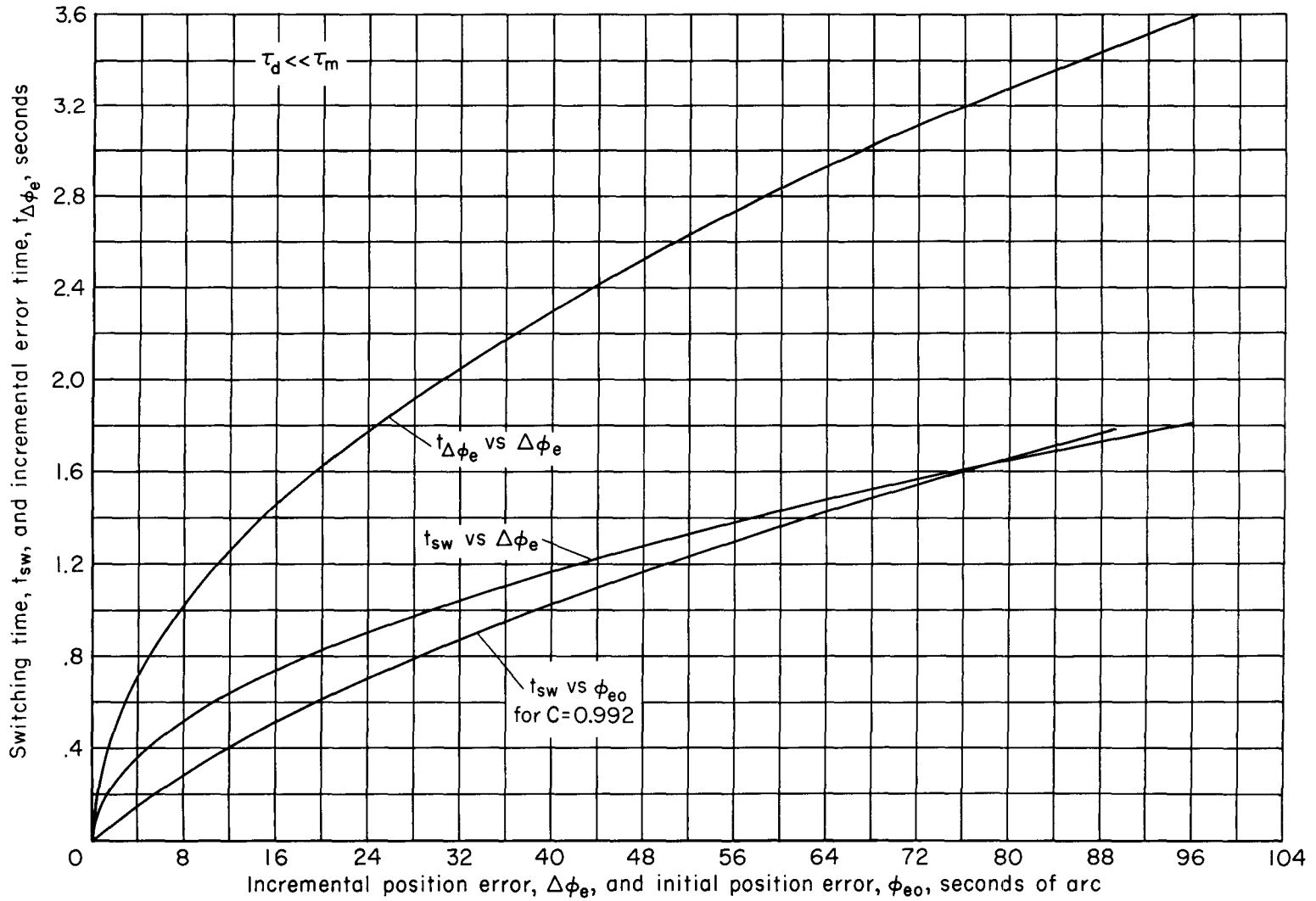

Figure 20.- Switching- and settling-time curves for rate-gyro and error-network systems.

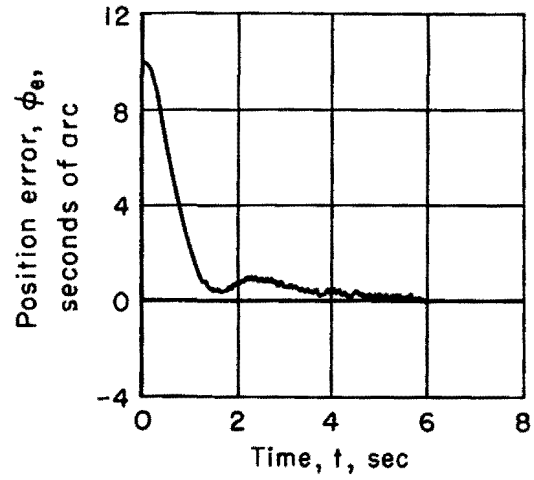

(a) Small-signal response.

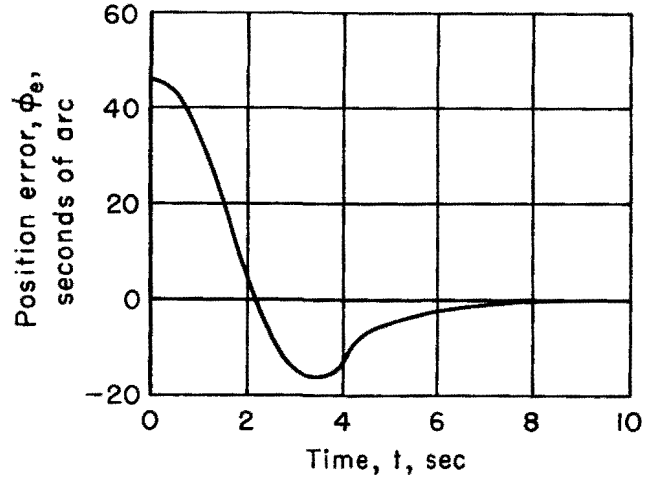

(b) Large-signal response.

Figure 21.- Small- and large-signal transient response curves for error-network system obtained by experimental testing.